

A VAE Approach to Sample Multivariate Extremes

Nicolas Lafon

*Laboratoire des Sciences du Climat et de l'Environnement
ESTIMR, CNRS-CEA-UVSQ
Gif-sur-Yvette, France*

NICOLAS.LAFON@LSCE.IPSL.FR

Philippe Naveau

*Laboratoire des Sciences du Climat et de l'Environnement
ESTIMR, CNRS-CEA-UVSQ
Gif-sur-Yvette, France*

PHILIPPE.NAVEAU@LSCE.IPSL.FR

Ronan Fablet

*IMT Atlantique, Lab-STICC
ODISSEY, INRIA
Brest, France*

RONAN.FABLET@IMT-ATLANTIQUE.FR

Abstract

Generating accurate extremes from an observational data set is crucial when seeking to estimate risks associated with the occurrence of future extremes which could be larger than those already observed. Applications range from the occurrence of natural disasters to financial crashes. Generative models from the machine learning (ML) community do not apply to extreme samples without careful adaptation. Besides, asymptotic results from extreme value theory (EVT) give a theoretical framework to model multivariate extreme events. Bridging these two fields, this paper details a variational autoencoder (VAE) approach for sampling multivariate heavy-tailed distributions, in which extremes of particularly large intensity are likely to occur. We illustrate the relevance of our approach on a synthetic data set and on a real data set of discharge measurements along the Danube river network. The latter shows the potential of our approach for flood risks' assessment. In addition to outperforming the vanilla VAE for the tested data sets, we also provide a comparison with a competing EVT-based generative approach. In the tested cases, our approach better captures the dependence structure between extreme events.

Keywords: multivariate extreme value theory, variational auto-encoders, generative models, neural network, environmental risk

1 Introduction

Simulating samples from an unknown distribution is a task that various studies have successfully tackled in the ML community during the past decade. This has led to the emergence of generative models, such as generative adversarial networks (GANs) (Goodfellow et al., 2020), VAEs (Kingma and Welling, 2013; Rezende et al., 2014), or normalizing flows (Rezende and Mohamed, 2015) (NFs). As ML tasks usually focus on average behaviors rather than rare events, these methods were originally not tailored to extrapolate upon the largest value of the training data set. This is a major shortcoming when dealing with extremes. Risk assessment in worst-case scenarios requires accurately sampling extremes

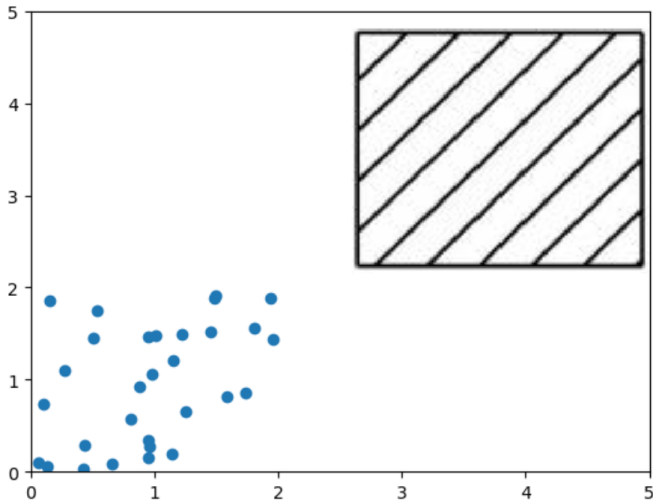


Figure 1: How to sample from observations (blue dots) in extreme regions (black square) to estimate probability of rare events?

at large quantiles, beyond the maximum values observed in the data set (Embrechts et al., 1999). Figure 1 illustrates this challenge with a two-dimensional case study: using a VAE approach, we aim, when relevant, to consistently generate samples in the extreme region (black square) from observations (blue dots), none of which lie within that region. In this context, EVT characterizes the probabilistic structure of extreme events and provides a theoretically-sound statistical framework to analyze them. A central concept in this framework is heavy-tail analysis (Resnick, 2007), which investigates phenomena where extreme values occur with non-negligible probability. Heavy-tailed distributions are thus particularly relevant in applications where rare but severe events play a crucial role. Data modeled by heavy-tailed distributions cover a wide range of application fields, e.g., hydrology (Anderson and Meerschaert, 1998; Rietsch et al., 2013), particle motion (Fortin and Clusel, 2015), finance (Bradley and Taqqu, 2003), Internet traffic (Hernandez-Campos et al., 2004), and risk management (Chavez-Demoulin and Roehrl, 2004; Das et al., 2013).

Recently, the intersection of ML and EVT has attracted growing attention. Several studies have highlighted the benefits of combining the two fields for diverse tasks. Beyond the generation of extremes, which is further discussed in the next paragraph, applications include dimensionality reduction (Drees and Sabourin, 2021), quantile function approximation (Pasche and Engelke, 2022), outlier detection (Rudd et al., 2017), and classification in tail regions (Jalalzai et al., 2018).

Related works: As demonstrated in Jaini et al. (2020); Huster et al. (2021), the output random variable of a neural network associated with a light-tailed input random variable cannot be heavy-tailed. This limitation has been the main motivation for adapting GANs and NFs to the sampling of heavy-tailed distributions. The main line of research relies

on introducing heavy-tailed latent variables. This strategy has been implemented through GANs with Pareto priors in Feder et al. (2020); Huster et al. (2021), as well as NFs with Student-t priors in Jaini et al. (2020); Laszkiewicz et al. (2022), the latter allowing for marginals with heterogeneous tail behaviors. A second approach treats marginal distributions and dependence structure separately. In Boulaguiem et al. (2022), the marginals are first estimated by fitting generalized Pareto distributions. To learn the dependence structure, the marginals are transformed to uniform distributions, and a GAN is trained in this transformed space, effectively capturing the copula representation (Embrechts, 2009). Another strategy targets the approximation of heavy-tailed quantile functions. Since neural networks with Rectified Linear Unit (ReLU) activations cannot directly map $[0, 1]$ to the quantile function of a heavy-tailed distribution, Allouche et al. (2022) proposed a GAN generator tailored to this mapping. Their results support the theoretical soundness of this approach for approximating true quantile functions. Finally, an empirical direction has been proposed in Bhatia et al. (2021), where GANs are recursively trained on tail samples to progressively reach a targeted return level.

Main contributions: To our knowledge, our study is the first attempt to bridge VAE and EVT. Recent studies suggest that state-of-the-art likelihood-based models, including VAEs, may, in some examples, capture the spread of the true distribution better than GANs (see, e.g., Razavi et al., 2019; Nash et al., 2021). This makes VAE an interesting way of explicitly exploiting the EVT framework to generate realistic and diverse extremes. Our main contributions are as follows:

- We first demonstrate that a VAE with standard parameterization cannot generate heavy-tailed distributions. We then propose a VAE framework to sample extremes from heavy-tailed distributions.
- Our approach can capture complex dependence structures between extremes by leveraging a polar representation of the data. It also enables direct sampling from the angular measure, which characterizes the asymptotic dependence between extremes (see Section 2.3)
- We illustrate the ability of our approach to generate realistic extremes in numerical experiments on both synthetic and real data sets, outperforming the Vanilla VAE and an EVT-based GAN approach (Huster et al., 2021).

Organization of the paper: In Section 2, we recall the basic principles of VAE and EVT. In Section 3, we present our main theoretical results concerning, on the one hand, the tail distribution of the marginals generated by a VAE and, on the other hand, the angular measure of generative models. All detailed proofs are delayed in Appendix G, listed in order of appearance in the paper. We detail the proposed VAE framework for multivariate extremes in Section 4 and describe the associated training setting in Section 5. Section 6 is dedicated to experiments. Section 7 is devoted to concluding remarks.

2 Background

In this section, we present background knowledge about VAE, and we give an introduction to univariate and multivariate heavy-tailed distributions.

2.1 VAE framework

To generate a sample from a random vector \mathbf{X} , a VAE relies on a two-step sampling strategy:

- A latent vector \mathbf{z} is drawn from a prior distribution $p_\alpha(\mathbf{z})$, parameterized by α ;
- A sample \mathbf{x} is then drawn from the conditional distribution $p(\mathbf{x} \mid \mathbf{z})$.

Since $p(\mathbf{x} \mid \mathbf{z})$ is in general not known, a parametric approximation $p_\theta(\mathbf{x} \mid \mathbf{z})$, referred to as the likelihood or probabilistic decoder, is introduced, with θ a set of learnable parameters. The aim is to find a parameterization that enables the generation of realistic samples of \mathbf{X} . To this end, the VAE framework introduces a variational distribution (or probabilistic encoder) $q_\phi(\mathbf{z} \mid \mathbf{x})$, parameterized by ϕ , to approximate the true posterior distribution $p(\mathbf{z} \mid \mathbf{x})$. Training then amounts to maximizing the evidence lower bound (ELBO) with respect to the parameters (α, ϕ, θ) . Formally, given N independent samples $(\mathbf{x}^{(i)})_{i=1}^N$ of \mathbf{X} , one has for each i ,

$$\log p(\mathbf{x}^{(i)}) \geq L(\mathbf{x}^{(i)}, \alpha, \theta, \phi),$$

where the ELBO L is defined as

$$L(\mathbf{x}^{(i)}, \alpha, \theta, \phi) = -D_{KL}\left(q_\phi(\mathbf{z} \mid \mathbf{x}^{(i)}) \parallel p_\alpha(\mathbf{z})\right) + \mathbb{E}_{q_\phi(\mathbf{z} \mid \mathbf{x}^{(i)})} \left[\log p_\theta(\mathbf{x}^{(i)} \mid \mathbf{z}) \right]. \quad (1)$$

The operator D_{KL} denotes the Kullback–Leibler (KL) divergence, defined for two distributions q and p by

$$D_{KL}(q \parallel p) = \int q(z) \log \left(\frac{q(z)}{p(z)} \right) dz,$$

which is always non-negative and equals zero if and only if $q = p$ almost everywhere. The ELBO over the whole data set is obtained by averaging Equation (1) over the N samples of \mathbf{X} .

To optimize the parameters (α, ϕ, θ) , Kingma and Welling (2013) and Rezende et al. (2014) introduced a training scheme that makes Equation (1) differentiable with respect to the parameters. First, the KL divergence term often admits a closed-form expression and is therefore easily differentiable with respect to (α, ϕ) . Second, the expectation in Equation (1) is approximated by an unbiased Monte Carlo estimator,

$$\frac{1}{L} \sum_{l=1}^L \log p_\theta(\mathbf{x}^{(i)} \mid \mathbf{z}^{(i,l)}),$$

where $\mathbf{z}^{(i,l)}$ are sampled from the random vector $\tilde{\mathbf{Z}}^{(i)}$ with distribution $q_\phi(\mathbf{z} \mid \mathbf{x}^{(i)})$. Differentiability is ensured by an explicit reparameterization, known as reparameterization trick, which introduces a function g_ϕ , differentiable with respect to ϕ , such that

$$\tilde{\mathbf{Z}}^{(i)} = g_\phi(\mathbf{x}^{(i)}, \mathcal{E}), \quad (2)$$

with \mathcal{E} a suitable random variable. Beyond ensuring differentiability, this reparameterization yields a low-variance estimator of the gradient, which is crucial for stable and efficient training. When explicit reparameterization is not feasible, implicit reparameterization can be employed (see Figurnov et al., 2018). Further details on implicit reparameterization are provided in Appendix F.

Example 1 *The most common parameterization of a VAE with $\mathbf{z} \in \mathbb{R}^n$ and $\mathbf{x} \in \mathbb{R}^m$ is*

$$\begin{aligned} p(\mathbf{z}) &= \mathcal{N}(\mathbf{z}; \mathbf{0}, \mathbf{I}_n), \\ p_\theta(\mathbf{x} \mid \mathbf{z}) &= \mathcal{N}(\mathbf{x}; \mu_\theta(\mathbf{z}), \text{diag}(\sigma_\theta(\mathbf{z}))^2), \\ q_\phi(\mathbf{z} \mid \mathbf{x}) &= \mathcal{N}(\mathbf{z}; \mu_\phi(\mathbf{x}), \text{diag}(\sigma_\phi(\mathbf{x}))^2), \end{aligned}$$

where μ_θ and σ_θ (resp. μ_ϕ and σ_ϕ) are neural network functions with parameters θ (resp. ϕ); $\text{diag}(\mathbf{v})$ denotes the diagonal matrix with the vector \mathbf{v} on its diagonal; and $\mathcal{N}(\mathbf{z}; \mu, \Sigma)$ is the pdf in variable \mathbf{z} of the multivariate normal distribution with mean μ and covariance matrix Σ . In this framework, the reparameterization trick takes the form

$$g_\phi(\mathbf{x}, \mathcal{E}) = \mu_\phi(\mathbf{x}) + \sigma_\phi(\mathbf{x}) \odot \mathcal{E},$$

where $\mathcal{E} \sim \mathcal{N}(\mathbf{0}, \mathbf{I}_n)$ and \odot denotes the element-wise product. In this case, the KL divergence of Equation (1) simplifies to

$$D_{KL}\left(q_\phi(\mathbf{z} \mid \mathbf{x}^{(i)}) \parallel p(\mathbf{z})\right) = \frac{1}{2} \sum_{j=1}^n \left(1 + 2 \log[\sigma_\phi(\mathbf{x}^{(i)})]_j - [\mu_\phi(\mathbf{x}^{(i)})]_j^2 - [\sigma_\phi(\mathbf{x}^{(i)})]_j^2\right),$$

where $[\mathbf{v}]_j$ is the j^{th} component of the vector \mathbf{v} .

We refer to this parameterization as the Standard VAE in the following.

2.2 Univariate Extremes

When modelling univariate extremes, generalized Pareto (GP) (Pickands III, 1975) distributions are of great interest. The GP survival function is defined for $\xi \in \mathbb{R}$ and $\sigma > 0$ by

$$\bar{H}_{\sigma, \xi}(x) = \left(1 + \xi \frac{x}{\sigma}\right)_+^{-1/\xi}, \quad (3)$$

where $a_+ = 0$ if $a < 0$. The scalar ξ is called the shape parameter. Note that Equation (3) is extended to $\xi = 0$, with $\bar{H}_{\sigma, 0}$ survival function of the exponential distribution of scale parameter σ .

Given a random variable X with cdf F , GP distributions appear under mild conditions as the simple limit of the threshold exceedance function $F_u(x) = P(X - u \leq x \mid X > u)$ when $u \rightarrow \infty$ (Balkema and De Haan, 1974). To be explicit, there exists $\xi \in \mathbb{R}$ and a strictly positive function $\sigma(\cdot)$ such that

$$\lim_{u \rightarrow x_F} \sup_{0 < x < x_F - u} |F_u(x) - H_{\sigma(u), \xi}(x)| = 0,$$

with $x_F = \sup\{x \text{ s.t. } F(x) < 1\}$ the right endpoint of F , and H the cdf of the GP distribution.

The shape parameter ξ of the GP approximation of F_u encompasses the information about the tail of X . In the following, we consider that:

- $\xi \leq 0$ corresponds to light-tailed distribution,
- $\xi > 0$ corresponds to heavy-tailed distribution.

Remark 1 A simple yet efficient way to sample from a GP distribution with parameters ξ and σ is to multiply an inverse gamma distributed random variable with shape $\frac{1}{\xi}$ and rate σ by a unit and independent exponential one. This multiplicative feature is essential for understanding the pivotal role of inverse-Gamma random variables in our sampling scheme in Section 4.2.

Remark 2 Notice that, given a light-tailed distribution with survival function \bar{F} , all its higher-order moments exist and are finite, and $\lim_{u \rightarrow \infty} u^a \bar{F}(u) = 0$ for any $a > 0$. In particular, Gaussian distributions are light-tailed. At the contrary, not all higher-order moments are finite for a heavy-tailed distribution.

In this work, we focus on heavy-tailed distributions, which can be seen as the distributions for which extremes have the greater intensity. The shape parameter governs the heaviness of a distribution's tail: the larger it is, the heavier the tail.

A final important notion regarding extreme values is the so-called regular variation property.

Definition 3 A random variable X is said to be regularly varying with tail index $\alpha > 0$, if

$$\lim_{t \rightarrow +\infty} P(X > tx \mid X > t) = x^{-\alpha}. \quad (4)$$

Importantly, X regularly varying equates to X heavy-tailed with $\alpha = \frac{1}{\xi}$ (see Bingham et al., 1989, Theorem 8.13.2).

2.3 Multivariate Extremes

By extending the notions developed in Section 2.2, a multivariate analogue of the GP distribution (Equation 3), referred to as multivariate GP, can be defined (see Rootzén and Tajvidi, 2006). Under mild conditions, the multivariate exceedance distribution asymptotically follows a multivariate GP distribution. Additionally, the regular variation of Definition 3 can be extended to a multivariate regular property (see, e.g. Resnick, 2007, for details). As in the univariate case, the convergence of exceedance distributions to a multivariate GP distribution and the property of multivariate regular variation are closely related. Thus, a multivariate random vector is heavy-tailed if it has multivariate regular variation.

Let \mathbf{X} be a random vector in $(\mathbb{R}^+)^m$. To define multivariate regular variation, we decompose \mathbf{X} into a radial component $R = X_1 + \dots + X_m = \|\mathbf{X}\|$ and an angular component of the $(m-1)$ -dimensional simplex $\Theta = \frac{\mathbf{X}}{\|\mathbf{X}\|}$.

Definition 4 \mathbf{X} has multivariate regular variation if the two following properties are fulfilled:

- The radius R is regularly varying as defined in Equation (4);
- There exists a probability measure \mathbf{S} defined on the $(m-1)$ -dimensional simplex such that (R, Θ) satisfies

$$P(\Theta \in \bullet \mid R > r) \xrightarrow{w} \mathbf{S}(\bullet), \quad (5)$$

where \xrightarrow{w} denotes weak convergence (see Appendix B.2). \mathbf{S} is called angular measure.

Consequently, the radius is a univariate heavy-tailed random variable as described in Section 2.2. The tail index of a multivariate regularly varying random vector is defined as the tail index of its radius. Besides, Equation (5) indicates that, if the radius is above a sufficiently high threshold, the respective distributions of the radius and the angle can be considered independent. Estimating the angular measure then becomes crucial to address tail events of the kind of $\{\mathbf{X} \in C\}$ for an ensemble C such that $u = \inf\{\|\mathbf{x}\|, \mathbf{x} \in C\}$ is large. This is especially true to assess the probability of joint extremes.

More generally, the estimation of the angular measure \mathbf{S} , although difficult due to the scarcity of examples (Cléménçon et al., 2021), is of great interest for the analysis of extreme values. In particular, it allows to determine confidence intervals for the probabilities of rare events (De Haan and De Ronde, 1998), bounds for probabilities of joint excesses over high thresholds (Engelke and Ivanovs, 2017) or tail quantile regions (Einmahl et al., 2013).

3 Tail properties of Distributions Sampled by Generative Models

Some important theoretical results are presented in this section. We first stress in Section 3.1 that the Standard VAE cannot generate heavy-tailed marginals. Then we focus on angular measures that can be obtained using generative models in Section 3.2. In particular, we prove that, when restricted to neural networks with ReLU activation functions, generative models based on the deterministic transformation of a prior input (e.g. GANs or NFs) have an angular measure concentrated on a restricted number of vectors. These theoretical considerations are crucial to define our VAE approach presented in Section 4.

3.1 Marginal Tail of a Standard VAE

In this section, we establish that a Standard VAE only produces light-tailed marginals. This result extends to VAEs results similar to those established for GANs with normal prior (see Huster et al., 2021), or with NFs with light-tailed base distribution (Jaini et al., 2020). We first mention an important property of neural networks, based on the notion of Lipschitz continuity (see Appendix B.1).

Proposition 5 (Arora et al., 2016; Huster et al., 2021): *A neural network $f : \mathbb{R}^n \rightarrow \mathbb{R}$ composed of operations such as ReLUs, leaky ReLUs, linear layers, maxpooling, maxout activation, concatenation or addition, is a piecewise linear operator with a finite number of linear regions. Therefore, f is Lipschitz continuous with respect to Minkowski distances.*

Given these elements, the following proposition describes the tail of a univariate output of a Standard VAE.

Proposition 6 *For the Standard VAE of Example 1 with univariate output ($m = 1$), given that the neural network functions μ_θ and σ_θ of the probabilistic decoder are piecewise linear operators, then the output distribution is light-tailed.*

Corollary 7 *The marginal distributions generated by the Standard VAE of Example 1 are light-tailed, whenever the neural networks functions μ_θ and σ_θ are composed of operations described in Proposition 5.*

3.2 Angular Measure of ReLu Networks Transformation of Random Vectors

In this section, we focus on the angular measures associated with generative models. We demonstrate that distributions sampled by algorithms based on the transformation of a random input vector through a ReLU neural network (a feed-forward network with linear layers and ReLU activation functions) have angular measures concentrated on a finite set of points on the simplex. Although not specific to VAEs, this result suggests a particular focus on the representation of the angular measure in the VAE framework.

Let us consider the following framework for generating multivariate heavy-tailed data in the non-negative orthant:

$$\mathbf{X} = f(\mathbf{Z}), \quad (6)$$

with \mathbf{Z} an n -dimensional input random vector with i.i.d heavy-tailed marginals and f a ReLU neural network with output in \mathbb{R}_+^m . This heavy-tailed sampling framework is used by Feder et al. (2020) and Huster et al. (2021) for GANs, and Jaini et al. (2020) for NFs. Within this framework \mathbf{X} is heavy-tailed with the same shape parameter as \mathbf{Z} , while it would be light-tailed if \mathbf{Z} were light-tailed.

In the limit of extreme values, one may ask which dependence structures between the marginals of \mathbf{X} can be represented by such a model. This corresponds to the angular measure defined in Equation (5). If we designate $\mathbf{S}_{\mathbf{X}}$ as the angular measure of \mathbf{X} , we can state the following Proposition.

Proposition 8 *Under the framework described in Equation (6), $\mathbf{S}_{\mathbf{X}}$ is concentrated on a finite set of points of the simplex less than n . In other words, it means that there exist some vectors $\{\mathbf{v}_1, \mathbf{v}_2, \dots, \mathbf{v}_{n'}\}$ with $n' \leq n$ such that for any subset \mathbb{A} of the $(m-1)$ -dimensional simplex*

$$\mathbf{S}_{\mathbf{X}}(\mathbb{A}) = \sum_{i=1}^{n'} p_i \delta_{\mathbf{v}_i}(\mathbb{A}),$$

where δ is the Dirac measure and $p_i > 0$ such that $\sum_{i=1}^{n'} p_i = 1$.

Informally, this proposition means that for sufficiently large radii, \mathbf{X} tends to concentrate along one of a finite set of direction vectors. While extracting certain principal directions in extreme regions is a useful tool for the comprehensive analysis of a data set (Drees and Sabourin, 2021), it is severely lacking in flexibility when it comes to represent more complex distributions and generate realistic extreme samples.

To circumvent this difficulty, we consider a polar decomposition of \mathbf{X} into radial and angular components, which are generated separately. This allows us to obtain angular measures that are more diverse than those concentrated on a finite set of vectors, as illustrated by the numerical experiments reported in Section 6.

4 Proposed VAE Architecture

4.1 Overall strategy

Our approach aims to adapt the VAE framework in order to generate multivariate regularly varying random vectors. To do so, the key principle of our approach is to separate the generation of the radius and of the angle. Following the polar decomposition $\mathbf{X} = R\Theta$, we

first aim to sample a heavy-tailed radius R , and then, conditionally on the sampled radius, to generate an angle Θ representing the dependence structure between the marginals. Thus we rely on two VAEs, the first one to sample the radius, the other one to sample the angle conditionally on the radius.

This separation allows us to model both the marginal tail behavior and the angular dependence of extremes in a flexible way, consistent with the theory of multivariate regular variation (Definition 4).

A major challenge lies in sampling a heavy-tailed radius. As shown in Proposition 6, the classical Gaussian parameterization of the VAE cannot generate heavy-tailed distributions. To overcome this limitation, we propose in Section 4.3 a new parameterization ensuring that the generated radius follows a heavy-tailed distribution. To provide intuition on how this parameterization works, Section 4.2 introduces a simplified multiplicative framework in which the resulting distributions are provably heavy-tailed (see Proposition 11).

Additionally, our aim is to represent rich and realistic angular measures on the simplex, avoiding their concentration on a few points, as is typically the case in the framework described in Proposition 8. This flexibility is naturally induced by the polar decomposition and is based on a conditional VAE that models the conditional distribution $\Theta \mid R$ (Section 4.4). In this conditional framework, we enforce asymptotic independence between the radius and the angle for large values of the radius, as required by multivariate regular variation, while enabling a diverse and smooth representation of the angular dependence at extreme levels.

To summarize, our strategy to generate a sample $\mathbf{x}^{(i)}$ of a multivariate regularly varying random vector is described by the following three-step VAE scheme:

- Using a VAE, a radius $r^{(i)}$ is drawn from a univariate heavy-tailed distribution R (see Section 4.3);
- Conditionally on the drawn radius $r^{(i)}$, we sample $\Theta^{(i)}$ an element of the $(m - 1)$ -dimensional simplex from the conditional distribution $\Theta \mid [R = r^{(i)}]$ while forcing the independence between radius R and angle Θ for large values of the radius. We use a conditional VAE for this purpose (see Section 4.4);
- We multiply componentwise the angle vector by the radius to obtain the desired sample, i.e. $\mathbf{x}^{(i)} = r^{(i)}\Theta^{(i)}$.

This generative strategy is illustrated in Figure 2.

4.2 Intuition Behind the Heavy-tailed Radius Sampling Scheme

Before detailing the specific parameterization that enables us to generate a heavy-tailed radius within a VAE framework, we first introduce a simplified multiplicative framework that guided our design choices and directly inspired the final formulation. The idea is to model the radius R through a heavy-tailed latent variable Z_{rad} , and to apply to it a very

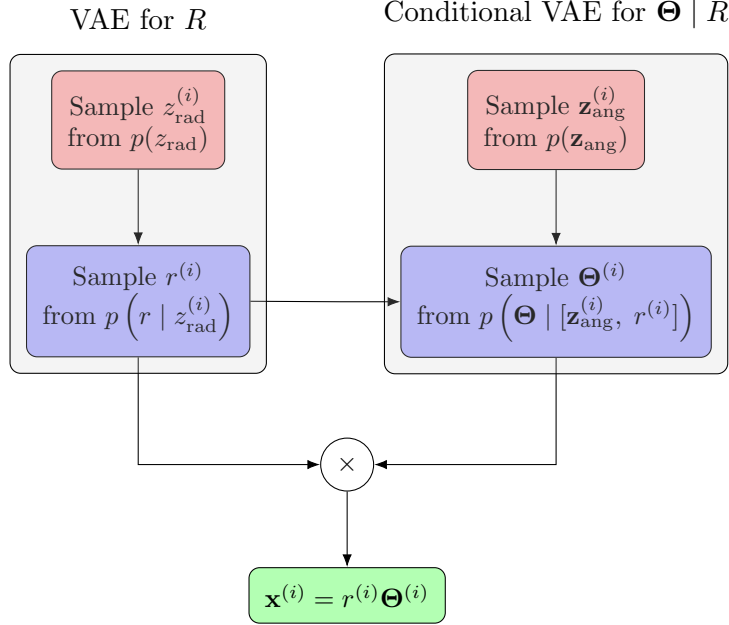


Figure 2: VAE scheme to draw a sample $\mathbf{x}^{(i)}$ (green block) from a multivariate regularly varying random vector. Two VAEs are involved (grey areas): one for radius generation (left) and one for angle generation (right). Each VAE relies on its own latent prior distribution (red blocks) and conditional distribution (blue blocks). Arrows indicate causal relations; the arrow between blue blocks shows that the angle is sampled conditionally on the radius.

simple transformation: namely, a multiplication by a lighter-tailed independent random variable. More precisely, we consider the following two conditions which, when satisfied, guarantee that the resulting radius is heavy-tailed.

Condition 9 Z_{rad} follows an inverse-gamma distribution defined for $z_{rad} > 0$ by the pdf

$$f_{\text{Inv}\Gamma}(z_{rad} ; \alpha, \beta) = \frac{\beta^\alpha}{\Gamma(\alpha)} z_{rad}^{-\alpha-1} \exp(-\beta/z_{rad}), \quad (7)$$

with α and β two strictly positive constants.

Condition 10 R is linked to Z_{rad} throughout a multiplicative model with a positive random coefficient A , i.e.

$$R = A \times Z_{rad},$$

where the random variable A is absolutely continuous and independent of Z_{rad} . We also assume that $0 < E[A^{\alpha+\epsilon}] < \infty$ for some positive ϵ .

We recall that the inverse-gamma distribution is heavy-tailed with tail index α and has a strictly positive support. Above, the moment condition $0 < E[A^{\alpha+\epsilon}] < \infty$ means that A

has a significantly lighter tail than Z_{rad} .

Under these two conditions, Breiman's lemma (Breiman, 1965) guarantees that the parameterization considered in Condition 10 leads to a heavy-tailed distribution of the radius R . Formally, the following proposition holds.

Proposition 11 *If Conditions 9 and 10 hold, R is heavy-tailed with tail index α . In particular, if A follows an exponential distribution with scale parameter c then R follows a GP distribution (see Equation 3 with $\xi = \frac{1}{\alpha}$ and $\sigma = \frac{\beta c}{\alpha}$)*

4.3 Sampling from Heavy-tailed Radius Distributions

The first component of our framework is a VAE designed to sample a heavy-tailed radius R . To tailor the VAE framework introduced in Section 2.1 to the sampling of heavy-tailed random variables, we set the prior Z_{rad} to follow inverse gamma distribution with parameters α and β , i.e. Z_{rad} satisfies Condition 9. Notice that if Z_{rad} follows an inverse gamma distribution with parameters α and β , then for each $c > 0$, cZ_{rad} is an inverse gamma with parameters α and $c\beta$. Consequently, and without loss of generality, we set parameter β of Z_{rad} equal to 1. Overall, we replace the light-tailed system described in Example 1 by the following heavy-tailed system:

$$p_\alpha(z_{rad}) = f_{\text{Inv}\Gamma}(z_{rad} ; \alpha, 1), \quad (8)$$

$$p_\theta(r | z_{rad}) = f_\Gamma(r ; \alpha_\theta(z_{rad}), \beta_\theta(z_{rad})), \quad (9)$$

$$q_\phi(z_{rad} | r) = f_{\text{Inv}\Gamma}(z_{rad} ; \alpha_\phi(r), \beta_\phi(r)), \quad (10)$$

with f_Γ the pdf of a Gamma distribution. $\alpha_\theta, \beta_\theta, \alpha_\phi, \beta_\phi$ are ReLU neural networks functions with parameters θ and ϕ . We may stress that the above parameterization ensures the non-negativeness of the samples both for the target and the likelihood.

The following proposition characterizes the heavy-tailed behavior of this univariate VAE scheme.

Proposition 12 *We consider the VAE parameterization described by Equations (8), (9) and (10). If we further assume that the function $\alpha_\theta(\cdot)$ is equal to a strictly positive constant, and the function $\beta_\theta(\cdot)$ satisfies*

$$\lim_{z_{rad} \rightarrow +\infty} \beta_\theta(z_{rad}) \propto \frac{1}{z_{rad}}, \quad (11)$$

$$\lim_{z_{rad} \rightarrow 0} \beta_\theta(z_{rad}) \propto \frac{1}{z_{rad}}, \quad (12)$$

then the univariate output distribution sampled by this VAE scheme is heavy-tailed with tail index equal to α .

In our implementation, we impose on $\beta_\theta(\cdot)$ to satisfy Equations (11) and (12) by choosing

$$\beta_\theta(z_{rad}) = \frac{|f_\theta(z_{rad})|}{z_{rad}^2}, \quad (13)$$

where f_θ is a ReLU neural network. Additionally, we allow $\alpha_\theta(\cdot)$ to be more flexible than a constant function, imposing only that it admits a strictly positive limit at infinity. This

corresponds to

$$\alpha_\theta(z_{rad}) = \frac{|g_\theta(z_{rad})|}{z_{rad}}, \quad (14)$$

where, again, g_θ is a ReLU neural network.

We choose our parameterization based on an analogy with the ideal multiplicative framework described in Section 4.1. Indeed, considering Conditions 9 and 10 verified, then

$$R \mid [Z_{rad} = z_{rad}] \stackrel{d}{=} Az_{rad}, \quad (15)$$

$$Z_{rad} \mid [R = r] \stackrel{d}{=} \frac{r}{A}. \quad (16)$$

Since A must have a lighter tail than Z_{rad} to satisfy the moment condition $E[A^{\alpha+\epsilon}] < \infty$ for some positive ϵ , we choose the approximate likelihood $p_\theta(r \mid z_{rad})$ in a light-tailed distribution family (i.e. Gamma distribution). Considering Equation (16), we notice that $Z_{rad} \mid [R = r]$ could be heavy-tailed if A have non-null probability on each open set containing 0. Thus we choose a heavy-tailed distribution for the target (i.e. Inverse-Gamma distribution). Additionally, as R and Z_{rad} are positive random variables, our parameterization ensures that negative values for either target and likelihood cannot occur.

Besides, by parameterizing both the prior p_α and the target q_ϕ as Inverse-Gamma distributions, the KL divergence in Equation (1) admits an analytical expression.

Proposition 13 *Given expression (8) and (10) for prior and target distributions, the KL divergence in Equation (1) is given by*

$$\begin{aligned} D_{KL}(q_\phi(z_{rad} \mid r) \parallel p_\alpha(z_{rad})) &= (\alpha_\phi(r) - \alpha)\psi(\alpha) - \log \frac{\Gamma(\alpha_\phi(r))}{\Gamma(\alpha)} \\ &\quad + \alpha \log \beta_\phi(r) + \alpha_\phi(r) \frac{1 - \beta_\phi(r)}{\beta_\phi(r)}, \end{aligned} \quad (17)$$

where Γ and ψ stands respectively for the gamma and digamma functions.

Interestingly, this proposition provides the basis for learning tail index α from data, which is a challenging issue in EVT (see, e.g. Danielsson et al., 2016).

4.4 Conditional Sampling of the Angle given the Radius

The second component of our overall framework is a conditional VAE (see, e.g., Zhao et al., 2017) which generates the angle given the previously sampled radius. More formally, it draws samples from the conditional distribution $\Theta \mid R$. This angular VAE has a multivariate normal prior \mathbf{Z}_{ang} . The target is also parameterized as a multivariate normal distribution, whose mean and standard deviation depend on both the latent variable and the radius. The likelihood is parameterized as a projection of a normal distribution on the \mathcal{L}_1 sphere. This projection is denoted Π , and is such that for any vector \mathbf{s} ,

$$\Pi(\mathbf{s}) = \frac{\mathbf{s}}{\|\mathbf{s}\|},$$

where the considered norm is the \mathcal{L}_1 -norm. Additionally, we define $\mathbf{S}(\Theta) = \{\mathbf{s}, \Pi(\mathbf{s}) = \Theta\}$. Overall, our conditional angular VAE relies on the following parameterization:

$$\begin{aligned} p(\mathbf{z}_{ang}) &= \mathcal{N}(\mathbf{z}_{ang} ; \mathbf{0}, \mathbf{I}_n), \\ p_\nu(\Theta | \mathbf{z}_{ang}, r) &= \int_{\mathbf{S}(\Theta)} \mathcal{N}(\mathbf{s} ; \mu_\nu(\mathbf{z}_{ang}, r), \text{diag}(\sigma_\nu(\mathbf{z}_{ang}, r))^2), \\ q_\omega(\mathbf{z}_{ang} | \Theta, r) &= \mathcal{N}(\mathbf{z}_{ang} ; \mu_\omega(\Theta, r), \text{diag}(\sigma_\omega(\Theta, r))^2), \end{aligned} \quad (18)$$

where n is the dimension of the latent space, $\mu_\nu, \sigma_\nu, \mu_\omega$ and σ_ω are neural network functions with parameters ν and ω . The dependence on R has been made explicit in both the target and the likelihood, thereby rendering the framework conditional.

As our initial aim is to sample on the multivariate simplex rather than on the multivariate sphere, we also use a Dirichlet parameterization of the likelihood. Details regarding this parameterization can be found in Appendix C.

To sample from multivariate regularly varying random vectors (Definition 4), we enforce the independence between the respective distributions of the radius and the angle when $r \rightarrow +\infty$ (see Equation (5)). To do so, we ensure that the functions μ_ν and σ_ν satisfy the following necessary condition.

Condition 14 μ_ν and σ_ν are such that there exist two z -varying functions μ_∞ and σ_∞ which verify for each \mathbf{z}_{ang}

$$\begin{aligned} \lim_{r \rightarrow +\infty} \mu_\nu(\mathbf{z}_{ang}, r) &= \mu_\infty(\mathbf{z}_{ang}), \\ \lim_{r \rightarrow +\infty} \sigma_\nu(\mathbf{z}_{ang}, r) &= \sigma_\infty(\mathbf{z}_{ang}). \end{aligned}$$

In our implementation, Condition 14 is enforced by imposing

$$\mu_\nu(\mathbf{z}_{ang}, r) = f_\nu \left(\mathbf{z}_{ang}, \frac{1}{1+r} \right), \quad (19)$$

$$\sigma_\nu(\mathbf{z}_{ang}, r) = g_\nu \left(\mathbf{z}_{ang}, \frac{1}{1+r} \right), \quad (20)$$

with f_ν and g_ν Lipschitz continuous neural networks.

Remark 15 From Equations (19) and (20), we deduce

$$\begin{aligned} \mu_\infty(\mathbf{z}_{ang}) &= f_\nu(\mathbf{z}_{ang}, 0), \\ \sigma_\infty(\mathbf{z}_{ang}) &= g_\nu(\mathbf{z}_{ang}, 0). \end{aligned}$$

Thus, sampling from the angular measure is an easy task as it is enough to: (i) draw sample \mathbf{z}_{ang} from the prior $\mathcal{N}(\mathbf{0}, \mathbf{I}_n)$, (ii) sample from $\mathcal{N}(\mu_\infty(\mathbf{z}_{ang}), \text{diag}(\sigma_\infty(\mathbf{z}_{ang}))^2)$, and (iii) project onto the \mathcal{L}_1 sphere through Π .

5 Implementation

This section introduces several implementation aspects of our approach. We first describe the architecture of the trained VAEs in Section 5.1, and then outline the learning set-up in Section 5.2. We also introduce in Section 5.3 performance metrics used for benchmarking purposes, and in Section 5.4 the approaches with which we compare the proposed VAE scheme.

5.1 Neural network parameterizations

In this section, we describe in detail the chosen parameterization of the neural architectures for the two VAEs introduced in Section 4, as used in the numerical experiments.

For the radius generation VAE described in Section 4.3, we consider ReLU neural networks with the following parameterizations:

- For the probabilistic encoder, we set two 5-dimensional hidden layers with ReLU activation. The output layer is a 2-dimensional dense layer with ReLU activation. For convergence purposes, we initialize the weights of the dense layers to 0 and their biases to a strictly positive value sampled from a uniform distribution between 1 and 2.
- For the probabilistic decoder, we detail the architecture of f_θ and g_θ of Equations (13) and (14). We consider the same architecture as the probabilistic encoder. Regarding the output, one corresponds to the output f_θ and the other one to the output of g_θ . The output bias of f_θ is initialized as a strictly positive value (randomly sampled from a uniform distribution between 1 and 2) and the output kernel of g_θ is initialized as a positive value (randomly sampled from a uniform distribution between 0.1 and 2).

For the angular VAE described in Section 4.4, the following parameterization are considered:

- For the encoder, the latent dimension is 4. We consider 3 hidden layers with ReLU activation, respectively with 8, 8 and 4 output features. The output layer is a dense linear layer. We use the default initialization scheme.
- For the decoder, the input radius is first transformed according to Equations (19) and (20). We use 3 hidden layers with ReLU activation, respectively with 5, 10 and 5 output features. The output layer is a dense layer. We use the default initialization scheme, except for the bias of the final layer, which is initially sampled from a uniform distribution between 0.5 and 3.

5.2 Learning Set-up

The considered training procedure follows from our hierarchical architecture with two VAEs and involves two distinct training losses, denoted by \mathcal{L}_R for the training loss of the radius VAE and $\mathcal{L}_{\Theta|R}$ for that of the angular VAE. For a data set $(\mathbf{x}^{(i)})_{i=1}^N$ with polar decomposition

$(r^{(i)}, \Theta^{(i)})$, we derive the training loss \mathcal{L}_R from Equations (1) and (17) as

$$\begin{aligned}\mathcal{L}_R(\alpha, \theta, \phi) = & \sum_{i=1}^N \left[\left((\alpha_\phi(r^{(i)}) - \alpha)\psi(\alpha) - \log \frac{\Gamma(\alpha_\phi(r^{(i)}))}{\Gamma(\alpha)} + \alpha \log \beta_\phi(r^{(i)}) + \alpha_\phi(r^{(i)}) \frac{1 - \beta_\phi(r^{(i)})}{\beta_\phi(r^{(i)})} \right) \right. \\ & \left. + \frac{1}{L} \sum_{l=1}^L \log f_\Gamma \left(r^{(i)} ; \alpha_\theta(z_{rad}^{(i,l)}), \beta_\theta(z_{rad}^{(i,l)}) \right) \right],\end{aligned}$$

Similarly, the training loss $\mathcal{L}_{\Theta|R}$ writes as

$$\begin{aligned}\mathcal{L}_{\Theta|R}(\nu, \omega) = & \sum_{i=1}^N \left[\frac{1}{2} \sum_{j=1}^n \left(1 + 2 \log[\sigma_\omega(\Theta^{(i)}, r^{(i)})]_j - [\mu_\omega(\Theta^{(i)}, r^{(i)})]_j^2 - [\sigma_\omega(\Theta^{(i)}, r^{(i)})]_j^2 \right) \right. \\ & \left. + \frac{1}{L} \sum_{l=1}^L \log \mathcal{N} \left(\Theta^{(i)} ; \mu_\nu(\mathbf{z}_{ang}^{(i,l)}, r^{(i)}), \text{diag}(\sigma_\nu(\mathbf{z}_{ang}^{(i,l)}, r^{(i)})^2) \right) \right].\end{aligned}$$

In the implementation of these training losses, we sample each $z_{rad}^{(i,l)}$ from the pdf $q_\phi(z_{rad} | r^{(i)})$, and each $\mathbf{z}_{ang}^{(i,l)}$ from the pdf $q_\omega(\mathbf{z}_{ang} | \Theta^{(i)}, r^{(i)})$. Overall, our training loss \mathcal{L}_{ExtVAE} is the sum

$$\mathcal{L}_{ExtVAE}(\alpha, \theta, \phi, \nu, \omega) = \mathcal{L}_R(\alpha, \theta, \phi) + \mathcal{L}_{\Theta|R}(\nu, \omega). \quad (21)$$

In practice, we first train the radius VAE, *i.e.* parameters (α, θ, ϕ) , and second the angular VAE, *i.e.* parameters (ν, ω) . Depending on the experiments, the parameter α of the radius prior can either be known or unknown. When known, it suffices to set α equal to the desired value in Equation (21). When unknown, α can be directly optimized by gradient descent. For estimating (α, θ, ϕ) , the training is limited to 5000 epochs, and the learning rate set to 10^{-4} . The same maximum number of epochs is used to estimate (ν, ω) but the learning rate is fixed to 10^{-5} .

In both cases, we used Adam optimizer (Kingma and Ba, 2014) and a batch size of 32. From a code perspective, we made extensive use of the Tensorflow and Tensorflow-Probability libraries. The whole code is freely available.¹

5.3 Performance Assessment

We present the various criteria used to evaluate the different approaches tested in our numerical experiments. These criteria can be grouped into three categories, depending on whether they relate to radius distributions, output distributions or angular measures.

For the radius distribution, log-quantile-quantile plots (for detailed examples, see Resnick, 2007, Chapter 4), abbreviated as log-QQ plots, are graphical methods we use to informally assess the goodness-of-fit of our model to data. This method consists in plotting the log of the empirical quantiles of a generated sample against those of the experimental data. If the fit is good, the plot should be roughly linear. We use the ELBO cost (Equation 1) on a given data set as a numerical indicator to compare the radius distribution obtained with our VAE approach to a vanilla VAE not tailored for extremes. Another criterion considered is

1. The implementation is available at <https://github.com/Nicolasecl16/ExtVAE>.

an estimator of the KL divergence between the data distribution and that generated by the tested approaches, together with a variant proposed by Naveau et al. (2014). This variant estimates the KL divergence above a specified threshold (see Appendix E.1).

For the whole set of generated samples, we investigate several other criteria. We compute the Wasserstein distances between extreme samples generated by the tested approaches and extreme true data samples. To do so, we select a large threshold u and compute the Wasserstein distance above this threshold by restricting the samples to points with a radius greater than u . Finally, we rescale this distance by dividing it by u^2 (see Appendix E.2). To compute the Wasserstein distances, we use pre-implemented functions from the Python Optimal Transport package (see Flamary et al., 2021).²

We have seen that for a multivariate regularly varying random vector, the radius and the angle becomes independent when the radius tends to infinity (see Equation 5). In practice, one can consider the radius and the angle independent by choosing a sufficiently large radius threshold. Wan and Davis (2019) have established a criterion to detect whether the respective distributions of the radius and the angle can be considered as independent, and thus to choose the corresponding threshold radius. This allows us to compare the threshold radii between the true data and the generated data. We rely on the testing framework introduced in Wan and Davis (2019) to calculate a p -value that follows a uniform distribution if the distributions of the radius and the angle are independent, and that is close to 0 otherwise (see Appendix E.3).

5.4 Notations and Benchmarked Approaches

We refer to our generative approach as ExtVAE if we assume that the tail index α is known, and as UExtVAE if the tail index is learned from data. If we restrict ourselves to the radii generated by ExtVAE and UExtVAE via the procedure described in Section 4.3, we denote respectively ExtVAE _{r} and UExtVAE _{r} . We compare our approach with the Standard VAE of Example 1, i.e. with normal distribution for prior, target and likelihood, indicated by the acronym StdVAE. We also compare our approach with ParetoGAN which is the GAN scheme for generating extremes proposed by Huster et al. (2021). The ParetoGAN is a Wasserstein GAN (see Arjovsky et al., 2017) with Pareto prior. Given the difficulty of training a GAN, as well as the number of factors that can influence the results it produces, we empirically tuned the ParetoGAN architecture to provide a sensible GAN baseline in our experiments. Although this parameterization may not be optimal, our interest goes beyond a simple quantitative intercomparison in exploring and understanding the differences between the proposed VAE approach and GANs in their ability to represent and sample extremes.

6 Experiments

We conduct experiments on synthetic and real multivariate data sets. The synthetic data set involves a heavy-tailed radius distribution and the angular distribution on the multivariate simplex is a Dirichlet distribution with radius-dependent parameters. The real data set corresponds to a monitoring of Danube river network discharges.

2. The documentation is available at <https://pythonot.github.io/quickstart.html>

Table 1: Mean ELBO cost (see Equation 1) computed on the training (Train), validation (Val) and test (Test) data set for the radius variable R_1 .

Approach	Train loss	Val loss	Test loss
StdVAE	1.21	4.81	$+\infty$
ExtVAE _r	0.88	1.10	1.12
UExtVAE _r	0.95	1.12	1.15

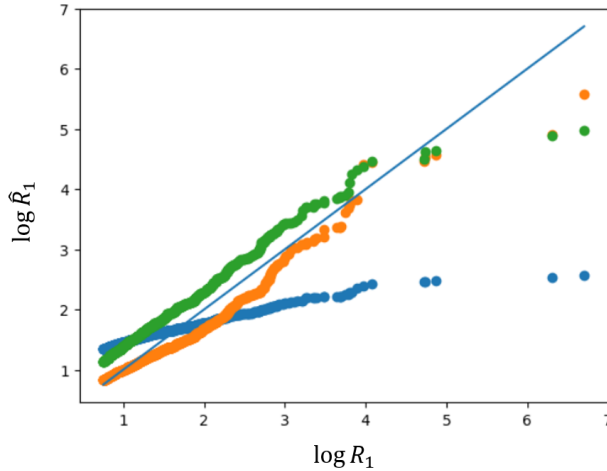


Figure 3: Log-QQ plot between the upper decile of 10000 radii samples from StdVAE (blue dots), ExtVAE_r (orange dots), UExtVAE_r (green dots) and the upper decile of the test data set of R_1 . The log values of the true radius, denoted $\log R_1$ is on the x-axis, the log of the estimated radius, denoted $\log \hat{R}_1$, is on the y-axis. The dots should lie close to the blue line

6.1 Synthetic Data Set

We first consider a synthetic data set of samples from a 5-dimensional heavy-tailed random vector with a tail index $\alpha = 1.5$. We detail the simulation setting in Appendix A.1. The training data set consists of 250 samples, compared to 750 for the validation data set and 10000 for the test data set.

In Table 1 and Figure 3, we study the ability of the benchmarked VAE schemes to sample heavy-tailed radius distribution. The results in Table 1 indicate that the mean ELBO cost remains approximately constant for our approaches across the training, validation, and test data sets, whereas it diverges for StdVAE. This indicates that our approaches, unlike StdVAE, successfully extrapolate the tail of the radius distribution. The log-QQ plots given in Figure 3 illustrate further that ExtVAE_r and UExtVAE_r schemes relevantly reproduce the tail pattern of the radius distribution R_1 while this is not the case for StdVAE. Figure 4 represents, for the compared methods, the evolution of the KL divergence between the true

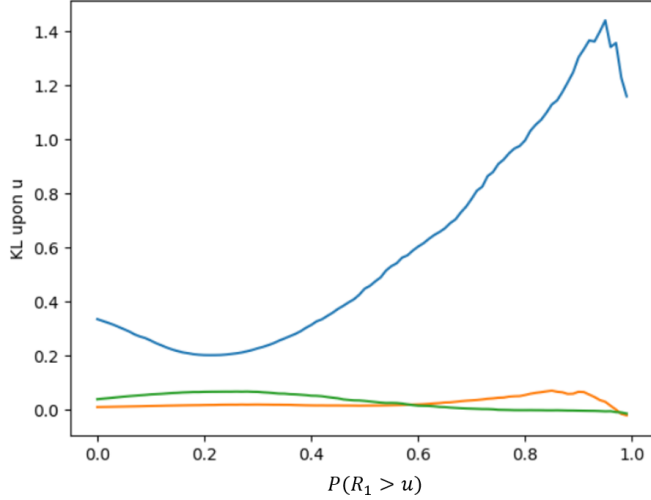


Figure 4: KL divergence between the radius distribution of the benchmarked VAE models and the target heavy-tailed distribution: we display the KL divergence (see Equation 26) above quantile u for $P(R_1 > u)$ varying from 0 to 1. The compared VAEs are the StdVAE (blue curve), the ExtVAE_r (orange curve) and the UEExtVAE_r (green curve). To estimate the KL divergences, 10,000 samples from each distribution are drawn, and u is set to the quantile computed from the samples of R_1 .

distribution and the simulated ones above a varying quantile u (Equation 26). Again, the StdVAE poorly matches the target distribution with a clear increasing trend for quantiles u such that $P(R_1 > u) \geq 0.3$. Conversely, the KL divergence is much smaller and much more stable for ExtVAE_r and UEExtVAE_r schemes, especially for large quantile values. Interestingly, for the different criteria, the results obtained with UEExtVAE_r are very close or even indistinguishable from those obtained with ExtVAE_r. This suggests that the estimation of the tail index is accurate. In order to better assess the robustness of this estimation, we report in Figure 5 the evolution of the tail index of UEExtVAE_r as a function of the training epochs for randomly chosen initial values. Given the expected uncertainty in estimating the tail index (see Appendix D), UEExtVAE_r estimates are globally consistent. We report meaningful estimation patterns since the reported curves tend to get closer to the true value as the number of epochs increase, although it might show some bias when initial value is far from the true tail index value. The mean value of the estimated tail index is 1.56 with a standard deviation of 0.2.

We now focus on the angle generation. The best parameterization for the likelihood of the conditional VAE is a Dirichlet parameterization (see Appendix C). An important advantage of our approach is the ability to generate samples on the simplex for a given radius as detailed in Section 4.4, and even to sample the angular measure. Figure 6 displays the angular measure projected onto the last two components of the simplex for the true angular measure, our ExtVAE approach and the ParetoGAN. For the latter, we approximate the angular measure by the empirical measure above a very high threshold. The ExtVAE

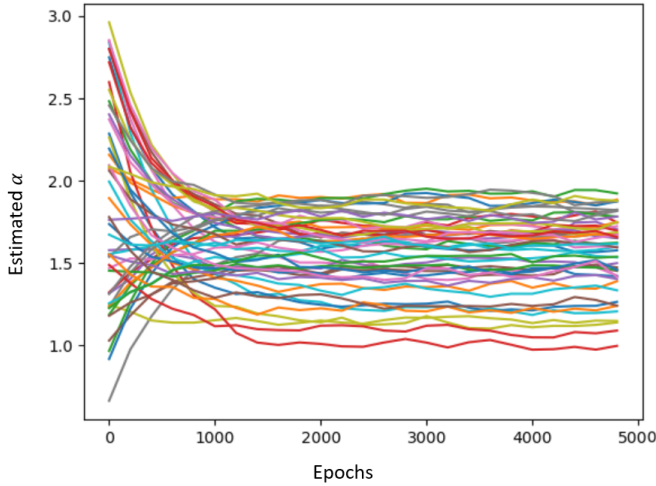


Figure 5: Evolution of the tail index α of UExtVAE_r during the training procedure: we report the value of the tail index as a function of the training epochs for training runs from different initial values. The initial values of α are sampled uniformly between 0.5 to 3. The true value of α is 1.5.

shows a good agreement with the true distribution, though not as sharp. By contrast, the distribution sampled by the ParetoGAN tends to reduce to a single mode. This confirms the result of Proposition 8.

To compare the overall distributions sampled by the the benchmarked schemes to the true data distribution, we estimate the Wasserstein distance (Equation 27) between 10000 generated items and the test set. The ExtVAE performs slightly better than the ParetoGAN (5.37 vs. 6.80). To compare the tails, Figure 7 shows the rescaled Wasserstein distance above a radius threshold (see Equation 28), computed between samples generated by the two approaches and the true data. We focus on radius thresholds above 2, which corresponds to the highest decile of the true data. Again, the ExtVAE performs better than the ParetoGAN, especially for radius values between 2 and 4, corresponding roughly to quantiles between 0.90 and 0.95. We recall that the ParetoGAN relies on the minimization of a Wasserstein metric, whereas the ExtVAE relies on a likelihood criterion. Therefore, we regard these results as an illustration of the better generalization performance of the ExtVAE, especially for the extremes.

At last, we estimate the threshold at which the radius and angle distributions become independent according to the criterion proposed by Wan and Davis (2019). Although, by construction, there is no radius value from which there is a true independence, the estimator gives a radius above which one can approximately consider that the limit measure is reached. We compare in Figure 8 the p -values for assessing independence between the radius distribution and the angle distribution (see Appendix E.3). The p -values are represented as a function of the chosen threshold for each of the three considered data sets: the test data set, the data set sampled from the ExtVAE and the data set sampled from the ParetoGAN. The ExtVAE slightly underestimates the radius threshold compared to

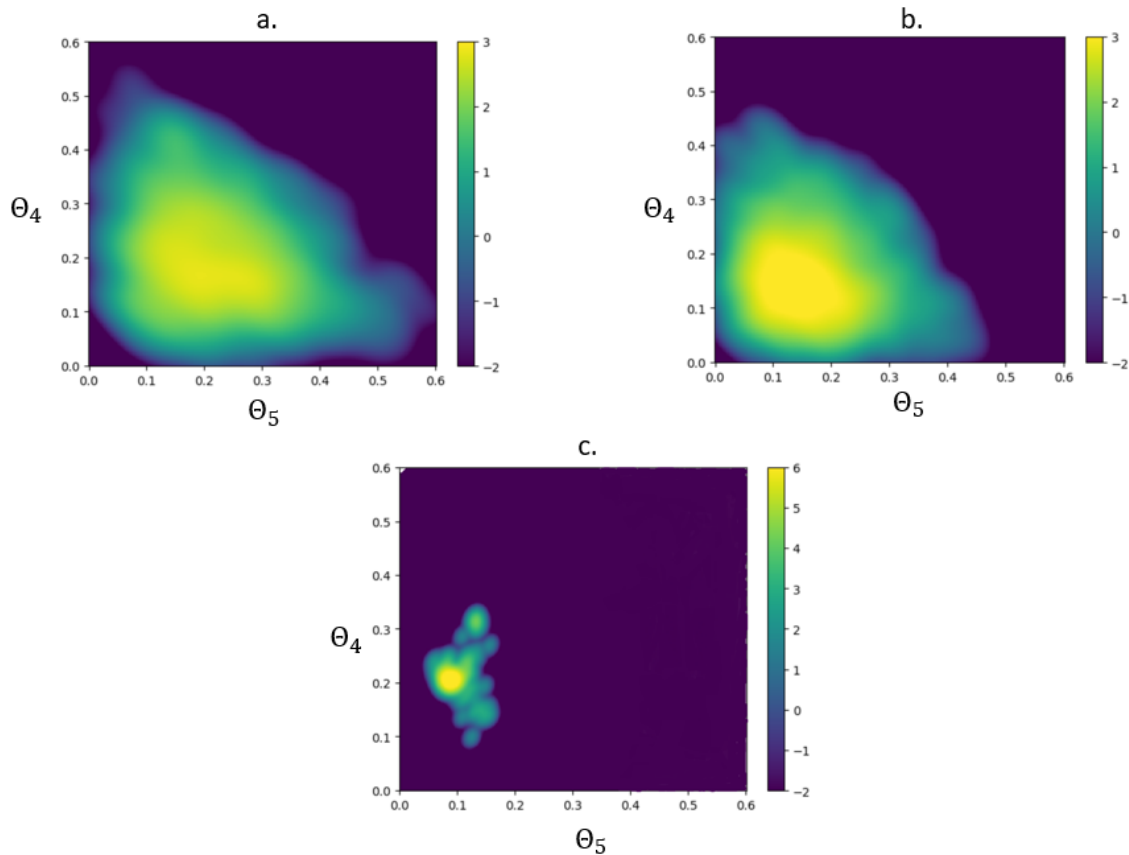


Figure 6: Log probability of the angular measure obtained with a. ExtVAE, b. true distribution, c. ParetoGAN, projected on axes 4 and 5 (named θ_4 and θ_5). For ParetoGAN, the estimation is based on 10000 samples at a high value of radius, typically above 10, which corresponds to the upper percentile of R_1 distribution.

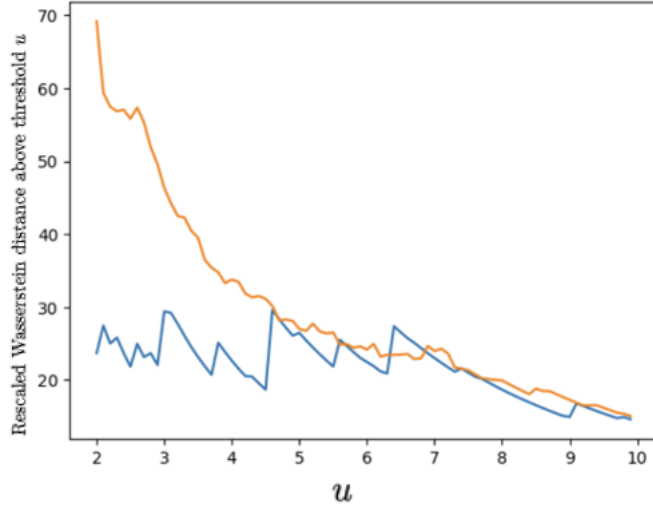


Figure 7: Wasserstein distance upon radius threshold u , divided by the square of u , calculated between 10000 samples drawn from generative models and test set. The ParetoGAN is shown in orange, and our model in blue. The considered thresholds are above 2, which is roughly the upper decile of the radius distribution.

the true data (1.3 vs. 1.6), while the ParetoGAN leads to a large overestimation (2.7 vs. 1.6). This illustrates further that the ExtVAE better captures the statistical features of high quantiles than ParetoGAN does. This improvement may be attributed to the polar decomposition used in the ExtVAE, which enables a more accurate modelling of the joint asymptotic behaviour of the radius and the angle.

6.2 Danube River Discharge Case-study

Our second experiment addresses a real heavy-tailed multivariate data set. We consider the daily time series of river flow measurements over 50 years at five stations (among thirty-one) of the Danube river network (see Appendix A.2 for further details). River flow data are known to often exhibit heavy-tailed behavior (see Katz et al., 2002). In reference to the numbering of the stations (see Figure 10), we note the random variables associated with the considered stations X_{23} , X_{24} , X_{25} , X_{26} , X_{27} . From the 50-year time series of daily measurements, we take a measurement every 25 days in the considered stations to form the training set. The remaining set serves as the test set. There are 730 daily measurements in the training set, and 17486 daily measurements in the test set. We have deliberately chosen a training set size that is significantly smaller than the test set size. This keeps the problem within the scope of tail extrapolation while retaining sufficient test data to reliably assess the accuracy of our tail distribution estimate.

We focus on the question raised in introduction (see Figure 1): can we extrapolate and generate consistent samples in extreme areas not observed during the training phase? We focus on extreme areas of the form $\bigcap_{i=23}^{27} X_i > u_i$ with u_i large predefined thresholds. This

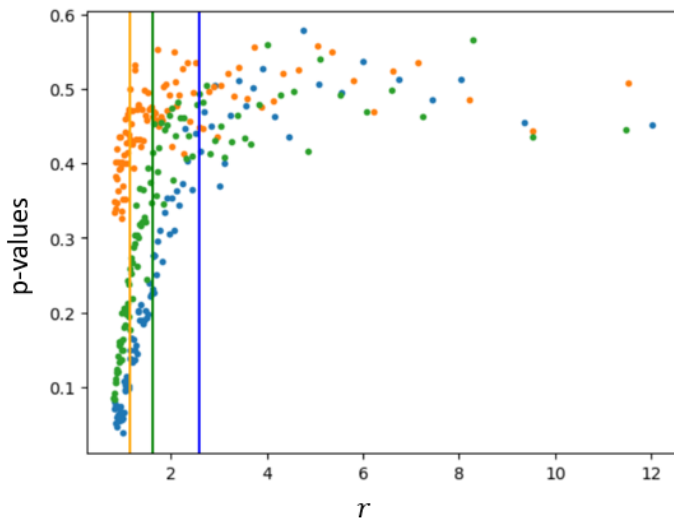


Figure 8: p -values for assessing independence between radius and angle distribution at different radius thresholds, computed according to Appendix E.3 for the test data set (green points), 10000 samples of the ExtVAE (orange points), and 10000 samples of the ParetoGAN (blue points). The vertical bars correspond to the threshold below which the p -values are less than 0.45. Above this threshold, the radius and the angle can be roughly considered as independent. We refer to Wan and Davis (2019) for further details.

corresponds to flows exceeding predefined thresholds at several stations. Namely we define

$$A_j^{(p)} = \bigcap_{i=23}^j X_i > u_i^{(p)}, \quad (22)$$

with p a given probability level and $u_i^{(p)}$ the corresponding quantile of the flow i in test set. The estimation of the probabilities of occurrence of such events is key to the assessment of major flooding risks along the river.

Our experiments proceed as follows. We train the StdVAE, the UExtVAE and the ParetoGAN using the training set. For this case-study, the best parameterization for the likelihood of the angular part of the UExtVAE is a projection of a multivariate normal distribution (see Equation 18). As evaluation framework, we generate for each trained model a number of samples of the size of the test data set, and we compare the proportion of samples that satisfy a given extreme event $A_j^{(p)}$ to that in the test data set. We consider extreme events $A_j^{(p)}$ with $p = 0.9$ and $p = 0.99$. Table 2 synthesizes this analysis for the StdVAE, UExtVAE and ParetoGAN. Note that the training data set does not include the considered extreme events when $p = 0.99$. Interestingly, the UExtVAE samples such extreme events with the same order of magnitude of occurrence as in the test data set. For instance, the proportion of samples that satisfy $A_{26}^{(0.99)}$ and $A_{27}^{(0.99)}$ is consistent with that observed in the test data set, respectively 0.2% and 0.18% against 0.4% and 0.25%. In contrast, the StdVAE does not generalize beyond the training data set. While it generates extreme events corresponding to $p = 0.9$, as these are present in the training data, it fails to produce any samples in $A_{26}^{(0.99)}$ and $A_{27}^{(0.99)}$. ParetoGAN generates samples that satisfy $A_{25}^{(0.99)}$, $A_{26}^{(0.99)}$ and $A_{27}^{(0.99)}$. Although satisfactory, the sampled proportions are further from true proportions than for our approach. Moreover, by repeating the experiment, it appears that $A_{25}^{(p)}$ is always equal to $A_{26}^{(p)}$ whenever $p \geq 0.9$. The effect is likely due to extremes being generated along a specific direction, as established in Proposition 8.

Because we study a true data set, the tail index of the radius of the discharge data set is not known a priori. Asadi et al. (2015) reports an estimate of 3.5 ± 0.5 considering only the summer months. In our case, the tail index of the trained UExtVAE is of 4.5. It is slightly higher than the value found by Asadi et al. (2015), which means a less heavy-tailed distribution. Indeed, half of the annual maxima occurs in June, July or August, typically due to heavy summer rain events. Thus, summer months are expected to depict heavier tails than the all-season data set, which is consistent with our findings.

7 Conclusion

This study bridges VAE and EVT to address the generative modeling of multivariate extremes. Following the concept of multivariate regular variation, we leverage a polar decomposition to combine a VAE for heavy-tailed radius sampling with a conditional VAE to sample from the angular distribution given the radius. Doing so, we explicitly address the dependence between the variables at each radius, and in particular the angular measure. Experiments performed on synthetic and real data support the relevance of our approach compared with vanilla VAE schemes and GANs tailored for extremes. In particular, we

Table 2: Proportion (in %) of extreme events $A_j^{(p)}$ (Equation 22) in the training and test data sets as well as in the data sets sampled from the trained StdVAE, UExtVAE and ParetoGAN with the same size as the test data set. The considered values of j are 25, 26 and 27, and those of p are 0.9 and 0.99.

	$p = 0.9$				
	Train	Test	UExtVAE	StdVAE	ParetoGAN
$A_{25}^{(p)}$	5.9	6.6	5.0	3.8	5.5
$A_{26}^{(p)}$	4.9	6.0	4.6	3.3	5.5
$A_{27}^{(p)}$	3.8	5.1	4.1	2.5	4.4

	$p = 0.99$				
	Train	Test	UExtVAE	StdVAE	ParetoGAN
$A_{25}^{(p)}$	0.0	0.48	0.22	0.01	0.13
$A_{26}^{(p)}$	0.0	0.4	0.2	0.0	0.13
$A_{27}^{(p)}$	0.0	0.25	0.18	0.0	0.09

illustrate the ability to consistently sample extreme regions that have never been observed during the training stage.

Our contribution naturally advocates for extensions to multivariate extremes in time and space-time processes (Basrak and Segers, 2009; Liu et al., 2012) as well as to VAE for conditional generation problems (Zheng et al., 2019; Grooms, 2021).

Acknowledgments and Disclosure of Funding

The authors acknowledge the support of the French Agence Nationale de la Recherche (ANR) under reference ANR-Melody (ANR-19-CE46-0011). Part of this work was supported by 80 PRIME CNRS-INSU, ANR-20-CE40-0025-01 (T-REX project), and the European H2020 XAIDA (Grant agreement ID: 101003469).

Appendix A. Data Sets

This appendix provides details on the two data sets used in the experiments. One data set is synthetic (A.1) and the other is a true data set compiling flow measurements (A.2).

A.1 Synthesized Data Sets

We sample in a space of dimension 5. The radius distribution R_1 is given by

$$R_1 = 2\mathbf{U} \times \mathbf{Inv}\Gamma(\alpha = 1.5 ; \beta = 0.6),$$

with \mathbf{U} uniformly distributed on $[0, 1]$. From Breiman's Lemma, the radius distribution is heavy-tailed with tail index $\alpha = 1.5$.

The detailed expression of the conditional angular distribution $\Theta_1 | R_1 = r$ is given by

$$[\Theta_1 | R_1 = r] = \mathbf{Diri}(a_1(r), a_1(r), a_2(r), a_2(r), a_2(r)), \quad (23)$$

where $a_1(r) = 3(2 - \min(1, 1/2r))$, $a_2(r) = 3(1 + \min(1, 1/2r))$, and **Diri** stands for Dirichlet distribution (see Appendix C).

Figure 9 gives the empirical pdf of R_1 based on 1000 samples.

A.2 Danube River Network Discharge Measurements

The Danube upper basin is a European river network which drainage basin covers a large part of Austria, Switzerland and southern Germany. Figure 10 shows the topography of the Danube basin as well as the locations of the 31 stations at which daily measurements of river discharge are available for a 50-year time period. Danube river network data set is available from the Bavarian Environmental Agency at <http://www.gkd.bayern.de>. As river discharges usually exhibit heavy-tailed distribution, this data set have been extensively studied in the community of multivariate extremes (see, e.g. Asadi et al., 2015; Mhalla et al., 2020). We consider measurements from a subset of five stations, numbered 23 to 27 (red triangles in Figure 10), from which we aim to generate new realistic observations.

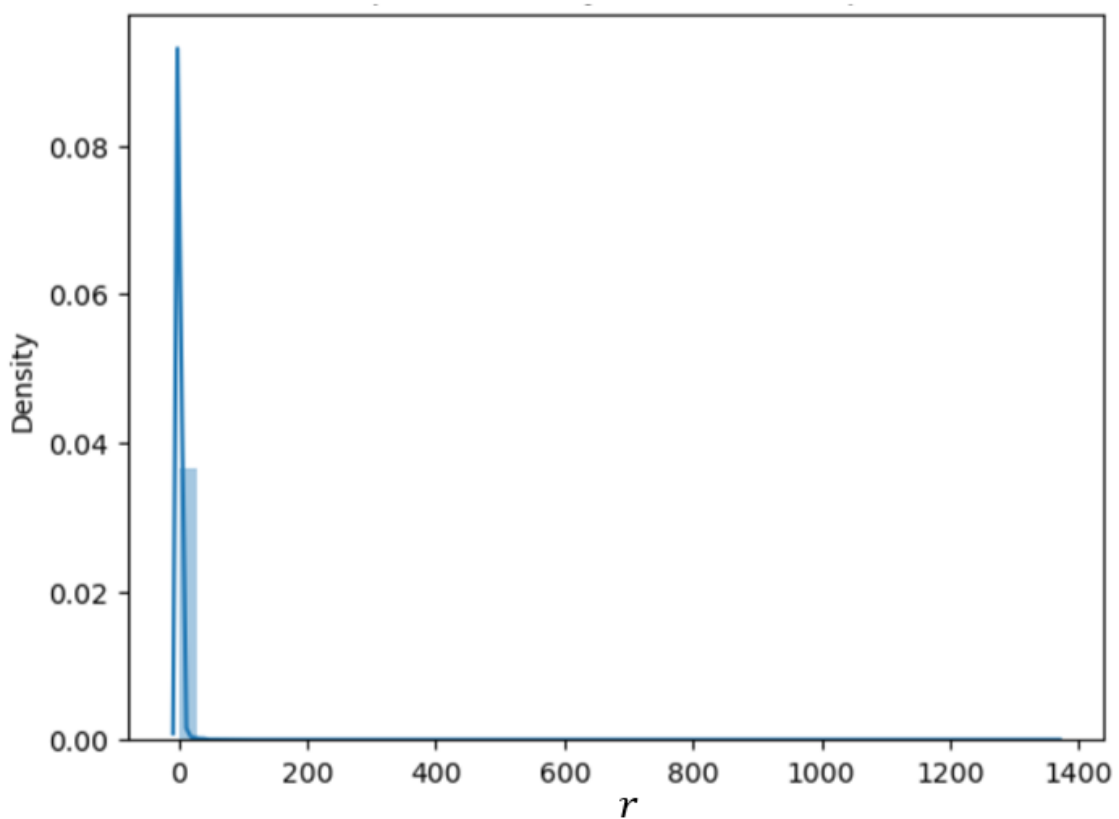
Appendix B. Additional Notions

This appendix provides further explanations of notions that are used either in the main text or in the proofs (Appendix G).

B.1 Lipschitz Continuity

Definition 16 *Let $(\mathbb{E}, d_{\mathbb{E}})$ and $(\mathbb{F}, d_{\mathbb{F}})$ be two metric spaces with $d_{\mathbb{E}}$ and $d_{\mathbb{F}}$ the respective metrics on sets \mathbb{E} and \mathbb{F} . A function $f : \mathbb{E} \rightarrow \mathbb{F}$ is called Lipschitz continuous if there exists a real constant $k \geq 0$ such that, for all x_1 and x_2 in \mathbb{E} ,*

$$d_{\mathbb{F}}(f(x_1), f(x_2)) \leq k d_{\mathbb{E}}(x_1, x_2). \quad (24)$$

Figure 9: Empirical density of R_1 based on 1000 samples.

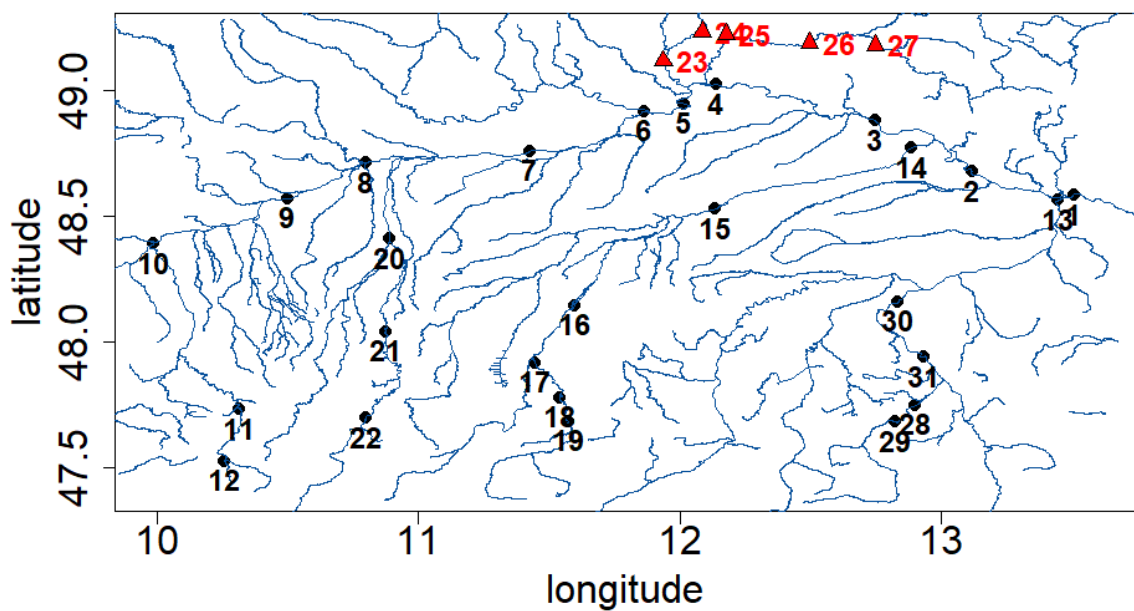


Figure 10: Topographic map of the upper Danube basin with 31 available gauging stations. In our experiments, we focus on the 5 stations indicated by the red triangles. A data set of 50 years of daily measurements is considered (from 1960 to 2010).

Remark 17 If \mathbb{E} and \mathbb{F} are normed vector spaces with respective norm $\|\cdot\|_{\mathbb{E}}$ and $\|\cdot\|_{\mathbb{F}}$, then f Lipschitz continuous implies that there exists $k \geq 0$ such that

$$d_{\mathbb{F}}(f(x), f(\mathbf{0}_{\mathbb{E}})) \leq k d_{\mathbb{E}}(x, \mathbf{0}_{\mathbb{E}}).$$

Consequently, $\|f(x)\|_{\mathbb{F}} \leq k\|x\|_{\mathbb{E}} + \|f(\mathbf{0}_{\mathbb{E}})\|_{\mathbb{F}}$.

B.2 Convergence of Measures

Definition 18 Let \mathbb{E} be a metric space and $(\mu_n)_{n \in \mathbb{N}}$ be a sequence of measures, then μ_n converges weakly to a measure μ as $n \rightarrow \infty$, if, for any $f : \mathbb{E} \rightarrow \mathbb{R}$ continuous real-valued bounded function,

$$\lim_{n \rightarrow \infty} \int_{\mathbb{E}} f d\mu_n = \int_{\mathbb{E}} f d\mu.$$

If this asymptotic result holds when f is continuous with compact support, we say that μ converges vaguely to μ_n , denoted \xrightarrow{v} . The vague convergence is equivalent to the convergence on all (relatively compact) continuity sets.

B.3 Additional definition of multivariate regular variation

The following definition of multivariate regularly varying vector extends Definition 4. We refer to Resnick (2007) Chapter 6 for a detailed review.

Definition 19 A random vector \mathbf{X} has multivariate regular variation if there exists a function $b \rightarrow \infty$ and a Radon measure $\mu_{\mathbf{X}}$ called the limit measure such that

$$\lim_{t \rightarrow \infty} t \mathbb{P} \left(\frac{\mathbf{X}}{b(t)} \in \bullet \right) \xrightarrow{v} \mu_{\mathbf{X}}(\bullet). \quad (25)$$

Note that this definition is slightly more general than Definition 19, as \mathbf{X} does not necessarily have positive components.

Remark 20 If the random vector \mathbf{X} has positive components, the angular measure $\mathbf{S}_{\mathbf{X}}$ defined in Equation (5) is directly related to the limit measure. Indeed, for any measurable subset \mathbb{A} of the simplex, and any measurable subset \mathbb{I} of $(0, \infty)$, it holds that

$$\mu_{\mathbf{X}} \circ T^{-1}(\mathbb{I}, \mathbb{A}) = \nu_{\alpha}(\mathbb{I}) \times \mathbf{S}_{\mathbf{X}}(\mathbb{A}),$$

where T is the polar transform define for any vector \mathbf{x} by $T(\mathbf{x}) = \left(\|\mathbf{x}\|, \frac{\mathbf{x}}{\|\mathbf{x}\|} \right)$, and ν_{α} a measure on $(0, \infty)$ such that $\nu_{\alpha}([t, \infty]) = ct^{-\alpha}$, with c and α strictly positive constants. Thus, the angular measure is the limit measure projected onto the simplex.

Appendix C. Dirichlet Parameterization of the Likelihood

A Dirichlet distribution with $m \geq 2$ strictly positive parameters $(a_i)_{i=1}^m$ is supported by the $(m-1)$ -dimensional simplex. Its pdf is defined by

$$f_{\text{Diri}}(\mathbf{x} ; (a_i)_{i=1}^m) = \frac{1}{B((a_i)_{i=1}^m)} \prod_{i=1}^m x_i^{a_i-1},$$

with $\mathbf{x} \in \mathbb{R}^m$ s.t $\sum_{i=1}^m x_i = 1$,

where B is the multivariate beta distribution.

To use a Dirichlet parameterization of the likelihood, Equation (18) becomes

$$p_\nu(\mathbf{s} \mid \mathbf{z}_{ang}, r) \sim f_{\text{Diri}}(\mathbf{s} ; a_\nu(\mathbf{z}_{ang}, r)),$$

where a_ν takes values in $(\mathbb{R}^+)^m$.

Using this parameterization, Condition 14 must be modified to preserve the asymptotic independence between the radius and angle distributions. It then takes the following form.

Condition 21 a_ν is such that there exists a function a_∞ which verifies for each \mathbf{z}_{ang}

$$\lim_{r \rightarrow +\infty} a_\nu(\mathbf{z}_{ang}, r) = a_\infty(\mathbf{z}_{ang}).$$

Again, we set $a_\nu(\mathbf{z}_{ang}, r) = h_\nu(\mathbf{z}_{ang}, \frac{1}{1+r})$, with h_ν Lipschitz continuous and $a_\infty(\mathbf{z}_{ang}) = h_\nu(\mathbf{z}_{ang}, 0)$. Similar to Remark 15, it is still easy to sample from the angular measure.

Appendix D. Tail Index Estimation

Estimating the tail index of a univariate distribution from samples is not an easy task. As an illustration, we drew the Hill plot (see e.g., Resnick (2007), Section 4.4; Xie (2017), Section 2.2) for R_1 in Figure 11. The Hill plot is based on the Hill estimator, which computes an estimate of the tail index from the k largest order statistics. Plotting this estimator as a function of k provides a graphical tool commonly used in the extreme-value community to assess the tail index. If the curve becomes approximately constant beyond a certain order statistic, this plateau value is taken as an estimate of the tail index. In our case, however, the Hill plot is difficult to interpret because no clear plateau emerges.

Other methods are also widely used to estimate the tail index, such as maximum likelihood estimation. This approach consists in fitting a GP distribution (Equation 3) to the subset of data exceeding a chosen threshold (see Coles et al., 2001, for details). For example, on the training dataset of R_1 , maximum likelihood estimation yields an estimate of 1.28 for the tail index when the threshold is the 0.8-quantile, but this estimate increases to 1.67 when using the 0.9-quantile as threshold.

Appendix E. Criteria

This section details the evaluation criteria used to benchmark the approaches in Section 6. These criteria assess (i) the radius distributions, with an emphasis on tail behavior (Appendix E.1), (ii) the similarity between the full multivariate distributions (Appendix E.2), and (iii) key statistics of the angular distributions (Appendix E.3).

E.1 KL Divergence upon Threshold

Let us assume that we have n samples $\mathcal{R}_{true} = (r_{true}^1, r_{true}^2, \dots, r_{true}^n)$ from the true radius distribution and m samples $\mathcal{R}_{gen} = (r_{gen}^1, r_{gen}^2, \dots, r_{gen}^m)$ from a generative model. Let \tilde{F}_{true} (respectively \tilde{F}_{gen}) denote the empirical estimator of the survival function of the true distribution (respectively the generated distribution) chosen to be non-zero above the largest

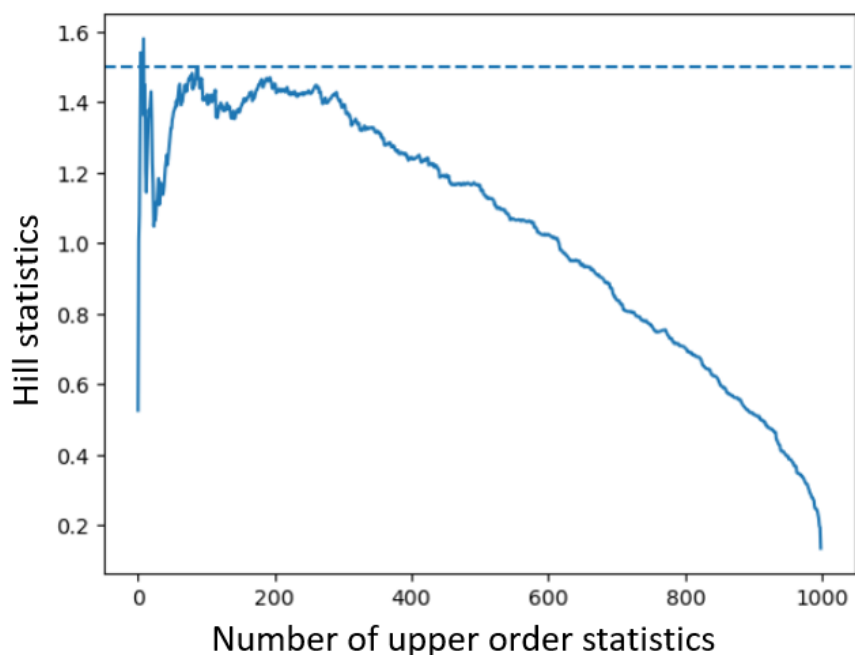


Figure 11: Hill plot for the 1000 R_1 samples of train and validation set (blue curve), the dashed line indicates the true value of the tail index, i.e. 1.5.

observed value. Then the empirical estimate $\text{KL}_u(\mathcal{R}_{\text{true}}, \mathcal{R}_{\text{gen}})$ of the KL divergence beyond a threshold u is given by

$$\begin{aligned} \text{KL}_u(\mathcal{R}_{\text{true}}, \mathcal{R}_{\text{gen}}) = & -1 - \frac{1}{N_n} \sum_{i=1}^m \log \left(\frac{\tilde{F}_{\text{gen}}(\max(r_{\text{gen}}^i, u))}{\tilde{F}_{\text{gen}}(u)} \right) \\ & -1 - \frac{1}{M_m} \sum_{i=1}^n \log \left(\frac{\tilde{F}_{\text{true}}(\max(r_{\text{true}}^i, u))}{\tilde{F}_{\text{true}}(u)} \right), \end{aligned} \quad (26)$$

where N_n and M_m are the number of samples above threshold u respectively among $\mathcal{R}_{\text{true}}$ and \mathcal{R}_{gen} .

E.2 Wasserstein Distance

Assume we have a set $\mathcal{X} = (\mathbf{x}_1, \dots, \mathbf{x}_n)$ of n i.i.d. samples from a random vector $\mathbf{X} \in \mathbb{R}^d$, and a set $\mathcal{Y} = (\mathbf{y}_1, \dots, \mathbf{y}_m)$ of m i.i.d. samples from a random vector \mathbf{Y} of the same dimension. We define $W(\mathcal{X}, \mathcal{Y})$ as the empirical Wasserstein distance between the empirical measures supported on \mathcal{X} and \mathcal{Y} :

$$W(\mathcal{X}, \mathcal{Y}) = \left(\min_{\gamma \in \mathbb{R}_+^{n \times m}} \sum_{i,j} \gamma_{i,j} \|\mathbf{x}_i - \mathbf{y}_j\|_2 \right)^{1/2}, \quad (27)$$

subject to

$$n\gamma \mathbf{1}_m = \mathbf{1}_n, \quad m\gamma^\top \mathbf{1}_n = \mathbf{1}_m,$$

where $\mathbf{1}_k$ denotes the k -dimensional vector of ones and $\|\cdot\|_2$ the Euclidean norm. The rescaled Wasserstein distance above a threshold r is defined by

$$W_r(\mathcal{X}, \mathcal{Y}) = \frac{W(\mathcal{X}_r, \mathcal{Y}_r)}{r^2}, \quad (28)$$

where $\mathcal{X}_r = \{\mathbf{x}_i \in \mathcal{X} : \|\mathbf{x}_i\|_2 > r\}$ and similarly \mathcal{Y}_r .

E.3 Threshold selection

Let us consider \mathbf{X} a random vector of \mathbb{R}^d with a polar decomposition (R, Θ) . Let $(\mathbf{x}_1, \mathbf{x}_2, \dots, \mathbf{x}_N)$ be a sequence of observed samples of \mathbf{X} with corresponding polar coordinates r_i and θ_i for each \mathbf{x}_i . Given a decreasing sequence of candidate thresholds for the radius $r_k^{(\text{ref})}$, the aim is to find the smallest $r_k^{(\text{ref})}$ such that R and Θ are independent given $R > r_k^{(\text{ref})}$. To assess independence between radius and angle distributions, Wan and Davis (2019) relies on the following hypothesis testing framework:

- H_0 : $R/r_k^{(\text{ref})}$ and Θ are independent given $R > r_k^{(\text{ref})}$,
- H_1 : $R/r_k^{(\text{ref})}$ and Θ are not independent given $R > r_k^{(\text{ref})}$.

Given these hypotheses, the authors propose a procedure for testing H_0 against H_1 , that yields a p -value uniformly distributed under H_0 and small under H_1 . Thus, for a given threshold r_k , when we average the p -values, we should find about 0.5 if H_0 is true and

closer to 0 when H_1 is true.

To compute the p -values, the authors rely on the empirical distance covariance (Székely et al., 2007).

Definition 22 *The empirical covariance between N observations $\mathcal{X} = \{\mathbf{x}_i\}_{i=1}^N$ and N observations $\mathcal{Y} = \{\mathbf{y}_i\}_{i=1}^N$ of two random vectors \mathbf{X} and \mathbf{Y} is given by*

$$T_N(\mathcal{X}, \mathcal{Y}) = \frac{1}{N^2} \sum_{i,j=1}^N \|\mathbf{x}_i - \mathbf{x}_j\|_2 \|\mathbf{y}_i - \mathbf{y}_j\|_2 + \frac{1}{N^4} \sum_{i,j,k,l=1}^N \|\mathbf{x}_i - \mathbf{x}_j\|_2 \|\mathbf{y}_k - \mathbf{y}_l\|_2 \\ - \frac{2}{N^3} \sum_{i,j,k=1}^N \|\mathbf{x}_i - \mathbf{x}_j\|_2 \|\mathbf{y}_i - \mathbf{y}_k\|_2,$$

with $\|\cdot\|_2$ the euclidean distance. Notice that \mathbf{X} and \mathbf{Y} have not necessarily equal sizes.

For a fixed threshold $r_k^{(ref)}$, the following data sets are considered,

$$(\mathcal{R}_{dep}, \Theta_{dep}) = \{(r_i, \theta_i) \text{ s.t. } r_i > r_k^{(ref)}, 1 \leq i \leq N\}, \\ \mathcal{R}_{indep} = \{r_i \text{ s.t. } r_i > r_k^{(ref)}, 1 \leq i \leq N\}, \\ \Theta_{indep} = \{\theta_i \text{ s.t. } r_i > r_k^{(ref)}, 1 \leq i \leq N\}.$$

We randomly choose a subsample of $(\mathcal{R}_{dep}, \Theta_{dep})$ of size N_k denoted $(\mathcal{R}_{dep}^{N_k}, \Theta_{dep}^{N_k})$. Then, we compute $T_{N,k} = T_{N_k}(\mathcal{R}_{dep}^{N_k}, \Theta_{dep}^{N_k})$, which is the empirical covariance between the radii and angles within the subsample.

To compute a p -value of $T_{N,k}$ under the assumption that the conditional empirical distribution is a product of the conditional marginals, we take a large number L of subsamples of size N_k of \mathcal{R}_{indep} on the one hand, and of Θ_{indep} on the other hand, respectively denoted $\mathcal{R}_{indep}^{N_k,l}$ and $\Theta_{indep}^{N_k,l}$ for $1 \leq l \leq L$. The empirical covariances $\{\tilde{T}_{N,k}^l\}_{l=1}^L = \{T_{N_k}(\mathcal{R}_{indep}^{N_k,l}, \Theta_{indep}^{N_k,l})\}_{l=1}^L$ between radii and angles can be computed.

The p -value pv_k of $T_{N,k}$ is the empirical value of $T_{N,k}$ relative the $\{\tilde{T}_{N,k}^l\}_{l=1}^L$, i.e.

$$pv_k = \frac{1}{L} \sum_{i=1}^L \mathbf{1}_{\mathbb{R}^+}(T_{N,k} - \tilde{T}_{N,k}^l),$$

with $\mathbf{1}_{\mathbb{R}^+}$ the indicator function of the set of positive real numbers.

This process is repeated m times, with different subsamples of $(\mathcal{R}_{dep}, \Theta_{dep})$ leading to m estimates of pv_k . The considered p -value is then the mean of these estimates. If the radius and angular distribution are independent, the p -value should be around 0.5, otherwise it is close to 0.

Appendix F. Implicit Reparameterization

When optimizing the ELBO cost given in Equation (1), explicit reparameterization (see Equation 2) is not feasible for the framework proposed in Section 4.3. Following Figurnov

et al. (2018), we therefore rely on an implicit reparameterization. It consists in differentiating the Monte Carlo estimator of $E_{q_\phi(Z|r^{(i)})}[f(Z)]$ using

$$\nabla_\phi E_{q_\phi(Z|r^{(i)})}[f(Z)] = -E_{q_\phi(Z|r^{(i)})}[\nabla_z f(z) \nabla_\phi F_{q_\phi}(z) (\nabla_z F_{q_\phi}(z))^{-1}],$$

with F_{q_ϕ} the cdf of q_ϕ . An implicit reparameterization of Gamma distribution, as well as inverse Gamma and many others, is available within a Tensorflow package named TensorflowProbability.³

Appendix G. Proofs

G.1 Proof of Proposition 6

In the standard parameterization described in Example 1, the prior and likelihood are given by

$$\begin{aligned} \mathbf{Z} &\sim \mathcal{N}(\mathbf{0}, \mathbf{I}_n), \\ X \mid [\mathbf{Z} = \mathbf{z}] &\sim \mathcal{N}(\mu_\theta(\mathbf{z}), \sigma_\theta(\mathbf{z})^2). \end{aligned}$$

The aim of the proof is to show that $\lim_{u \rightarrow +\infty} u^a P(X > u) = 0$ for all $a > 0$, in accordance with Remark 2.

The survival function of X is given by

$$\begin{aligned} P(X > u) &= \int_{\mathbf{z}} P(X > u \mid \mathbf{Z} = \mathbf{z}) p(\mathbf{z}) d\mathbf{z} \\ &= \int_{\mathbf{z}} \left(\int_u^{+\infty} \frac{1}{\sqrt{2\pi\sigma_\theta(\mathbf{z})^2}} \exp\left(-\frac{(x - \mu_\theta(\mathbf{z}))^2}{2\sigma_\theta(\mathbf{z})^2}\right) dx \right) p(\mathbf{z}) d\mathbf{z} \\ &= \int_{\mathbf{z}} \frac{1}{2} \operatorname{erfc}\left(\frac{u - \mu_\theta(\mathbf{z})}{\sqrt{2}\sigma_\theta(\mathbf{z})}\right) p(\mathbf{z}) d\mathbf{z}, \end{aligned}$$

where erfc is the complementary error function defined for $y \in \mathbb{R}$ by $\operatorname{erfc}(y) = 1 - \frac{2}{\sqrt{\pi}} \int_0^y e^{-t^2} dt$.

Letting $\Omega(u) = \{\mathbf{z} \in \mathbb{R}^n \text{ s.t. } u - \mu_\theta(\mathbf{z}) > 0\}$, the previous expression could also be written

$$\begin{aligned} P(X > u) &= \int_{\mathbf{z} \in \Omega(u)} \frac{1}{2} \operatorname{erfc}\left(\frac{u - \mu_\theta(\mathbf{z})}{\sigma_\theta(\mathbf{z})}\right) p(\mathbf{z}) d\mathbf{z} \\ &\quad + \int_{\mathbf{z} \in \overline{\Omega(u)}} \frac{1}{2} \operatorname{erfc}\left(\frac{u - \mu_\theta(\mathbf{z})}{\sigma_\theta(\mathbf{z})}\right) p(\mathbf{z}) d\mathbf{z}, \\ &= f_1(u) + f_2(u). \end{aligned}$$

3. Details could be found at <https://www.tensorflow.org/probability>

Notice first that $f_2(u) \leq P(\mathbf{z} \in \overline{\Omega(u)})$. As μ_θ is Lipschitz continuous, there exists constants $k > 0$ and $b \in \mathbb{R}$ such that $\mu_\theta(\mathbf{z}) \leq k\|\mathbf{z}\| + b$ (see Remark 17).

It implies that, for $u > b$,

$$\begin{aligned} f_2(u) &\leq P\left(\|\mathbf{z}\| \geq \frac{u-b}{k}\right) \\ &\leq \frac{1}{2} \operatorname{erfc}\left(\frac{u-b}{\sqrt{2}k}\right) \\ &\leq \exp\left(-\left(\frac{u-b}{\sqrt{2}k}\right)^2\right). \end{aligned} \quad (29)$$

where we have used the inequality (Chiani et al., 2003)

$$\operatorname{erfc}(y) \leq e^{-y^2}, \text{ for } y > 0. \quad (30)$$

From Equation (29), we obtain $\lim_{u \rightarrow +\infty} u^a f_2(u) = 0$.

To obtain a similar result for f_1 , we again use inequality (30) to obtain

$$f_1(u) \leq \int_{\mathbf{z} \in \Omega(u)} \exp\left(-\left(\frac{u - \mu_\theta(\mathbf{z})}{\sqrt{2}\sigma_\theta(\mathbf{z})}\right)^2\right) p(\mathbf{z}) d\mathbf{z}.$$

As σ_θ is Lipschitz continuous, there exist constants $k' > 0$ and $b' \in \mathbb{R}$ such that $\sqrt{2}\sigma_\theta(\mathbf{z}) \leq k'\|\mathbf{z}\| + b'$. Then, we can state that

$$f_1(u) \leq \int_{\mathbf{z} \in \Omega(u)} \exp\left(-\left(\frac{u - (k'\|\mathbf{z}\| + b')}{k't + b'}\right)^2\right) p(\mathbf{z}) d\mathbf{z}. \quad (31)$$

For any given $a > 0$, we define the real-valued function

$$g_u(t) = u^a \exp\left(-\left(\frac{u - (kt + b)}{k't + b'}\right)^2\right).$$

The following holds :

$$\lim_{u \rightarrow +\infty} g_u(t) = 0.$$

Additionally, $g_u(t)$ is maximized with respect to u when $u = u^*(t)$ with

$$u^*(t) = \frac{-(kt + b) + \sqrt{(kt + b)^2 + 4a(k't + b')^2}}{2}.$$

Thus, we obtain

$$|g_u(t)| \leq (2\sqrt{a}(k't + b'))^a,$$

which leads to

$$|g_u(\|\mathbf{z}\|)p(\mathbf{z})| \leq (2\sqrt{a}(k'\|\mathbf{z}\| + b'))^a \exp(-\|\mathbf{z}\|^2/2).$$

Since the quantity on the right-hand is integrable with respect to $\|\mathbf{z}\|$ and independent of u , it follows by the dominated convergence theorem and Equation (31) that $\lim_{u \rightarrow +\infty} u^a f_1(u) = 0$.

The previous results yield $\lim_{u \rightarrow +\infty} u^a P(X > u) = \lim_{u \rightarrow +\infty} u^a (f_1(u) + f_2(u)) = 0$. From Remark 2, we therefore conclude that X is light-tailed.

G.2 Proof of Proposition 8

In this proof, we make extensive use of the limit measure of a multivariate regularly varying vector introduced in Definition 19. Recall from Remark 20 that, when the components of a random vector are non-negative, the angular measure defined in Equation (5) is the projection of its limit measure onto the simplex. Consequently, to prove that the angular measure is supported by finitely many points of the simplex, it is sufficient to show that the limit measure is concentrated on finitely many direction vectors.

Step 1: Limit measure of the prior. First, the limit measure $\mu_{\mathbf{Z}}$ of \mathbf{Z} is concentrated on the coordinate axes. More precisely,

$$\mu_{\mathbf{Z}} \left(\mathbb{R}^n \setminus \bigcup_{i=1}^n \{t\mathbf{e}_i : t > 0\} \right) = 0,$$

where \mathbf{e}_i denotes the i -th canonical basis vector of \mathbb{R}^n (with a 1 in the i -th position and 0 elsewhere). As shown in (Resnick, 2007, Section 6.5), this follows from the i.i.d. nature of the components of \mathbf{Z} .

Step 2: Effect of linear transformations. The following lemma describes how the limit measure behaves under multiplication by a matrix.

Lemma 23 *Let \mathbf{Y} be a d -dimensional regularly varying random vector whose limit measure is supported on the finite set of direction vectors $\bigcup_{i=1}^{n'} \{t\mathbf{v}_i : t > 0\}$. For any $m \times d$ matrix \mathbf{W} , the transformed vector \mathbf{WY} is also regularly varying, and its limit measure is supported on*

$$\bigcup_{i=1}^{n'} \{t\mathbf{Wv}_i : t > 0\},$$

excluding those indices i for which $\mathbf{Wv}_i = \mathbf{0}$. In particular, the limit measure of \mathbf{WY} is supported on at most n' direction vectors.

Proof It follows from

$$t \mathbb{P} \left(\frac{\mathbf{WY}}{b(t)} \in \bullet \right) = t \mathbb{P} \left(\frac{\mathbf{Y}}{b(t)} \in \mathbf{W}^{-1}(\bullet) \right) \xrightarrow{v} \mu_{\mathbf{Y}}(\mathbf{W}^{-1}(\bullet)) =: \mu_{\mathbf{WY}}(\bullet),$$

that \mathbf{WY} is regularly varying.

If $\mu_{\mathbf{Y}}$ is supported on $\{t\mathbf{v}_i\}$, then $\mu_{\mathbf{Y}} \circ \mathbf{W}^{-1}(\mathbb{A}) > 0$ implies $\mathbf{W}^{-1}(\mathbb{A}) \cap \{t\mathbf{v}_i\} \neq \emptyset$, hence $\mathbb{A} \cap \{t\mathbf{Wv}_i\} \neq \emptyset$, provided $\mathbf{Wv}_i \neq \mathbf{0}$. Thus the support of $\mu_{\mathbf{WY}}$ is precisely the set of nonzero images \mathbf{Wv}_i . ■

Step 3: Effect of adding a bias.

Lemma 24 *If the d -dimensional vector \mathbf{Y} has multivariate regular variation with limit measure $\mu_{\mathbf{Y}}$, then for any d -dimensional vector \mathbf{b} , the shifted vector $\mathbf{Y} + \mathbf{b}$ is also regularly varying, with the same limit measure. Hence, if $\mu_{\mathbf{Y}}$ is supported on finitely many direction vectors, the same holds for the limit measure of $\mathbf{Y} + \mathbf{b}$.*

Proof Write $\varepsilon_t = \mathbf{b}/b(t) \rightarrow 0$. Let \mathbb{A} be a relatively compact continuity set, bounded away from the origin. Then

$$t \mathbb{P}\left(\frac{\mathbf{Y} + \mathbf{b}}{b(t)} \in \mathbb{A}\right) = t \mathbb{P}\left(\frac{\mathbf{Y}}{b(t)} \in \mathbb{A} - \varepsilon_t\right).$$

Define for $\delta > 0$ the sets

$$\mathbb{A}^{-\delta} := \{x : x + u \in \mathbb{A} \text{ for all } u, \|u\| \leq \delta\}, \quad \mathbb{A}^{+\delta} := \{x : \text{dist}(x, \mathbb{A}) \leq \delta\}.$$

When $\|\varepsilon_t\| \leq \delta$,

$$\mathbb{A}^{-\delta} \subset \mathbb{A} - \varepsilon_t \subset \mathbb{A}^{+\delta}.$$

Using the vague convergence of the rescaled measures $t \mathbb{P}\left(\frac{\mathbf{Y}}{b(t)} \in \bullet\right)$ to $\mu_{\mathbf{Y}}$, we obtain, letting $t \rightarrow \infty$,

$$\mu_{\mathbf{Y}}(\mathbb{A}^{-\delta}) \leq \liminf_{t \rightarrow \infty} t \mathbb{P}\left(\frac{\mathbf{Y} + \mathbf{b}}{b(t)} \in \mathbb{A}\right) \leq \limsup_{t \rightarrow \infty} t \mathbb{P}\left(\frac{\mathbf{Y} + \mathbf{b}}{b(t)} \in \mathbb{A}\right) \leq \mu_{\mathbf{Y}}(\mathbb{A}^{+\delta}).$$

Since $\mu_{\mathbf{Y}}(\partial\mathbb{A}) = 0$ and \mathbb{A} is bounded away from 0, the regularity of Radon measures ensures that $\mu_{\mathbf{Y}}(\mathbb{A}^{\pm\delta}) \rightarrow \mu_{\mathbf{Y}}(\mathbb{A})$. Hence the limit measure is preserved. \blacksquare

Step 4: Effect of the ReLU activation. Let $\text{ReLU}(x) = \max(x, 0)$ applied componentwise. If the limit measure of \mathbf{Y} is supported on $\{tv_i\}$, then the limit measure of $\text{ReLU}(\mathbf{Y})$ is supported on the directions

$$\{t \text{ReLU}(v_i) : t > 0\}.$$

If v_i has at least one negative coordinate, the corresponding coordinate in $\text{ReLU}(v_i)$ becomes 0, potentially collapsing the direction. Thus ReLU can only reduce the number of supporting direction vectors.

Step 5: Conclusion for neural networks. A ReLU neural network consists of successive applications of:

- multiplication by weight matrices,
- addition of biases,
- ReLU nonlinearities.

By iterating Lemmas 23–24 and the ReLU argument, the limit measure remains concentrated on finitely many direction vectors at every layer. Since the output has non-negative coordinates, its angular measure is supported by a finite set of points of the simplex. Moreover, the number of such points is bounded above by the input dimension n .

This completes the proof.

G.3 Proof of Proposition 11

Consider an exponential distribution A , with scale parameter c , and Z_{rad} an inverse-gamma distribution with parameters (α, β) . The cdf of R is given by

$$\begin{aligned}
P(R \leq t) &= \int_0^{+\infty} P(A \leq z) \times \frac{t}{z^2} f_{\text{Inv}\Gamma} \left(\frac{t}{z} ; \alpha, \beta \right) dz, \\
&= 1 - \frac{\beta^\alpha}{t^\alpha \Gamma(\alpha)} \int_0^{+\infty} z^{\alpha-1} e^{-\frac{z}{c}} e^{-\frac{\beta z}{t}} dz, \\
&= 1 - \frac{\beta^\alpha}{t^\alpha} \left(\frac{1}{c} + \frac{\beta}{t} \right)^{-\alpha}, \\
&= 1 - \left(1 + \frac{t}{\beta c} \right)^{-\alpha}, \\
&= 1 - \bar{H}_{\sigma, \xi}(t),
\end{aligned}$$

with $\sigma = \frac{\beta c}{\alpha}$ and $\xi = \frac{1}{\alpha}$. Consequently, R follows a generalized Pareto distribution. Notice that we use the change of variable $u = z \left(\frac{1}{c} + \frac{\beta}{t} \right)$ from the second to the third line of the above equations.

G.4 Proof of Proposition 12

The aim of this proof is to show that the radius R sampled by the VAE is heavy-tailed with tail index α . We first establish that there exists $\gamma > 0$ such that $E[R^\gamma] = \infty$, implying that R is necessarily heavy-tailed, in accordance with Remark 2. We then argue that the only possible value of the tail index is α .

The pdf of R is given by

$$\begin{aligned}
p(r) &= \int_0^{+\infty} p_\theta(r | z_{rad}) p_\alpha(z_{rad}) dz_{rad}, \\
&= \int_0^{+\infty} f(r, z_{rad}) dz_{rad},
\end{aligned}$$

with

$$f(r, z_{rad}) = f_{\Gamma}(r ; \alpha_\theta(z_{rad}), \beta_\theta(z_{rad})) f_{\text{Inv}\Gamma}(z_{rad} ; \alpha, 1).$$

Since α_θ is equal to a constant denoted a_θ , it leads to the expression

$$f(r, z_{rad}) = \frac{r^{a_\theta-1}}{\Gamma(\alpha)\Gamma(a_\theta)} z_{rad}^{-(\alpha+1)} \beta_\theta(z_{rad})^{a_\theta} e^{-r\beta_\theta(z_{rad}) - \frac{1}{z_{rad}}}.$$

From Equations (11) and (12), we can state the existence of m and M two strictly positive constants such that, for any z ,

$$\frac{m}{z} \leq \beta_\theta(z) \leq \frac{M}{z}.$$

Consequently,

$$f_1(r, z_{rad}) \leq f(r, z_{rad}) \leq f_2(r, z_{rad})$$

with

$$\begin{aligned} f_1(r, z_{rad}) &= \frac{r^{a_\theta-1}}{\Gamma(\alpha)\Gamma(a_\theta)} z_{rad}^{-(a_\theta+\alpha+1)} m^{a_\theta} e^{-r \frac{M}{z_{rad}} - \frac{1}{z}}, \\ f_2(r, z_{rad}) &= \frac{r^{a_\theta-1}}{\Gamma(\alpha)\Gamma(a_\theta)} z_{rad}^{-(a_\theta+\alpha+1)} M^{a_\theta} e^{-r \frac{m}{z_{rad}} - \frac{1}{z}}. \end{aligned}$$

We can obtain analytical expressions of $\int_0^{+\infty} f_1(r, z_{rad}) dz_{rad}$ and $\int_0^{+\infty} f_2(r, z_{rad}) dz_{rad}$,

$$\begin{aligned} \int_0^{+\infty} f_1(r, z_{rad}) dz_{rad} &= \frac{r^{a_\theta-1} m^{a_\theta}}{\Gamma(\alpha)\Gamma(a_\theta)} \int_0^{+\infty} z_{rad}^{-(a_\theta+\alpha+1)} e^{-r \frac{M}{z_{rad}} - \frac{1}{z}} dz_{rad}, \\ &= \frac{r^{a_\theta-1} m^{a_\theta}}{\Gamma(\alpha)\Gamma(a_\theta)} \Gamma(a_\theta + \alpha) (1 + rM)^{-a_\theta - \alpha}, \end{aligned}$$

where we used the change of variables $u = \frac{1+rM}{z_{rad}}$. Using same arguments, we also obtain

$$\int_0^{+\infty} f_2(r, z_{rad}) dz_{rad} = \frac{r^{a_\theta-1} M^{a_\theta}}{\Gamma(\alpha)\Gamma(a_\theta)} \Gamma(a_\theta + \alpha) (1 + rm)^{-a_\theta - \alpha}.$$

It leads to these asymptotic results when $r \rightarrow \infty$,

$$\begin{aligned} \int_0^{+\infty} f_1(r, z_{rad}) dz_{rad} &\propto r^{-\alpha-1}, \\ \int_0^{+\infty} f_2(r, z_{rad}) dz_{rad} &\propto r^{-\alpha-1}. \end{aligned}$$

Consequently, $E[R^\gamma]$ is infinite whenever $\gamma > \alpha$. R is necessarily heavy-tailed. Since $E[R^\gamma]$ is finite for $\gamma < \alpha$, the only possible value of the tail index of R is α (see Embrechts et al., 1999, Proposition A.38 (d)).

G.5 Proof of Proposition 13

Let $\alpha_1, \alpha_2, \beta_1$ and β_2 be strictly positive constants. The following holds.

$$\begin{aligned} D_{KL}(f_{\text{Inv}\Gamma}(z; \alpha_1, \beta_1) \parallel f_{\text{Inv}\Gamma}(z; \alpha_2, \beta_2)) &= E_{z \sim \text{Inv}\Gamma(\alpha_1, \beta_1)} \left[\log \left(\frac{f_{\text{Inv}\Gamma}(z; \alpha_1, \beta_1)}{f_{\text{Inv}\Gamma}(z; \alpha_2, \beta_2)} \right) \right] \\ &= E_{y \sim \Gamma(\alpha_1, \beta_1)} \left[\log \left(\frac{f_{\text{Inv}\Gamma}(\frac{1}{y}; \alpha_1, \beta_1)}{f_{\text{Inv}\Gamma}(\frac{1}{y}; \alpha_2, \beta_2)} \right) \right] \\ &= E_{y \sim \Gamma(\alpha_1, \beta_1)} \left[\log \left(\frac{f_{\Gamma}(y; \alpha_1, \beta_1)}{f_{\Gamma}(y; \alpha_2, \beta_2)} \right) \right] \\ &= D_{KL}(f_{\Gamma}(z; \alpha_1, \beta_1) \parallel f_{\Gamma}(z; \alpha_2, \beta_2)). \end{aligned} \quad (32)$$

Equation (17) holds from Equation (32) and the following result (Penny et al., 2006):

$$\begin{aligned} D_{KL}(f_{\Gamma}(z; \alpha_1, \beta_1) \parallel f_{\Gamma}(z; \alpha_2, \beta_2)) &= (\alpha_1 - \alpha_2) \psi(\alpha_1) - \log \frac{\Gamma(\alpha_1)}{\Gamma(\alpha_2)} \\ &\quad + \alpha \log \frac{\beta_1}{\beta_2} + \alpha_1 \frac{\beta_2 - \beta_1}{\beta_1}. \end{aligned}$$

References

Michaël Allouche, Stéphane Girard, and Emmanuel Gobet. Ev-gan: Simulation of extreme events with relu neural networks. *Journal of Machine Learning Research*, 23(150):1–39, 2022.

Paul L Anderson and Mark M Meerschaert. Modeling river flows with heavy tails. *Water Resources Research*, 34(9):2271–2280, 1998.

Martin Arjovsky, Soumith Chintala, and Léon Bottou. Wasserstein generative adversarial networks. In *International conference on machine learning*, pages 214–223. PMLR, 2017.

Raman Arora, Amitabh Basu, Poorya Mianjy, and Anirbit Mukherjee. Understanding deep neural networks with rectified linear units. *arXiv preprint arXiv:1611.01491*, 2016.

Peiman Asadi, Anthony C Davison, and Sebastian Engelke. Extremes on river networks. *The Annals of Applied Statistics*, 9(4):2023–2050, 2015.

August A Balkema and Laurens De Haan. Residual life time at great age. *The Annals of probability*, 2(5):792–804, 1974.

Bojan Basrak and Johan Segers. Regularly varying multivariate time series. *Stochastic processes and their applications*, 119(4):1055–1080, 2009.

Siddharth Bhatia, Arjit Jain, and Bryan Hooi. Exgan: Adversarial generation of extreme samples. In *Proceedings of the AAAI Conference on Artificial Intelligence*, volume 35, pages 6750–6758, 2021.

Nicholas H Bingham, Charles M Goldie, Jozef L Teugels, and JL Teugels. *Regular variation*. Number 27. Cambridge university press, 1989.

Younes Boulaguiem, Jakob Zscheischler, Edoardo Vignotto, Karin van der Wiel, and Sebastian Engelke. Modeling and simulating spatial extremes by combining extreme value theory with generative adversarial networks. *Environmental Data Science*, 1, 2022.

Brendan O Bradley and Murad S Taqqu. Financial risk and heavy tails. In *Handbook of heavy tailed distributions in finance*, pages 35–103. Elsevier, 2003.

Leonard Breiman. On some limit theorems similar to the arc-sin law. *Theory of Probability & Its Applications*, 10(2):323–331, 1965.

Valérie Chavez-Demoulin and Armin Roehrl. Extreme value theory can save your neck. *ETHZ publication*, 2004.

Marco Chiani, Davide Dardari, and Marvin K Simon. New exponential bounds and approximations for the computation of error probability in fading channels. *IEEE Transactions on Wireless Communications*, 2(4):840–845, 2003.

Stéphan Clémençon, Hamid Jalalzai, Stéphane Lhaut, Anne Sabourin, and Johan Segers. Concentration bounds for the empirical angular measure with statistical learning applications. *arXiv preprint arXiv:2104.03966*, 2021.

Stuart Coles, Joanna Bawa, Lesley Trenner, and Pat Dorazio. *An introduction to statistical modeling of extreme values*, volume 208. Springer, 2001.

Jon Danielsson, Lerby Murat Ergun, Laurens de Haan, and Casper G de Vries. Tail index estimation: Quantile driven threshold selection. *Available at SSRN 2717478*, 2016.

Bikramjit Das, Paul Embrechts, and Vicky Fasen. Four theorems and a financial crisis. *International Journal of Approximate Reasoning*, 54(6):701–716, 2013.

Laurens De Haan and John De Ronde. Sea and wind: multivariate extremes at work. *Extremes*, 1:7–45, 1998.

Holger Drees and Anne Sabourin. Principal component analysis for multivariate extremes. *Electronic Journal of Statistics*, 15(1):908–943, 2021.

John HJ Einmahl, Laurens de Haan, and Andrea Krajina. Estimating extreme bivariate quantile regions. *Extremes*, 16(2):121–145, 2013.

Paul Embrechts. Copulas: A personal view. *Journal of Risk and Insurance*, 76(3):639–650, 2009.

Paul Embrechts, Sidney I Resnick, and Gennady Samorodnitsky. Extreme value theory as a risk management tool. *North American Actuarial Journal*, 3(2):30–41, 1999.

Sebastian Engelke and Jevgenijs Ivanovs. Robust bounds in multivariate extremes. 2017.

Richard M Feder, Philippe Berger, and George Stein. Nonlinear 3d cosmic web simulation with heavy-tailed generative adversarial networks. *Physical Review D*, 102(10):103504, 2020.

Mikhail Figurnov, Shakir Mohamed, and Andriy Mnih. Implicit reparameterization gradients. *Advances in neural information processing systems*, 31, 2018.

Rémi Flamary, Nicolas Courty, Alexandre Gramfort, Mokhtar Z Alaya, Aurélie Boisbunon, Stanislas Chambon, Laetitia Chapel, Adrien Corenflos, Kilian Fatras, Nemo Fournier, et al. Pot: Python optimal transport. *J. Mach. Learn. Res.*, 22(78):1–8, 2021.

Jean-Yves Fortin and Maxime Clusel. Applications of extreme value statistics in physics. *Journal of Physics A: Mathematical and Theoretical*, 48(18):183001, 2015.

Ian Goodfellow, Jean Pouget-Abadie, Mehdi Mirza, Bing Xu, David Warde-Farley, Sherjil Ozair, Aaron Courville, and Yoshua Bengio. Generative adversarial networks. *Communications of the ACM*, 63(11):139–144, 2020.

Ian Grooms. Analog ensemble data assimilation and a method for constructing analogs with variational autoencoders. *Quarterly Journal of the Royal Meteorological Society*, 147(734):139–149, 2021.

Felix Hernandez-Campos, JS Marron, Gennady Samorodnitsky, and F Donelson Smith. Variable heavy tails in internet traffic. *Performance Evaluation*, 58(2-3):261–284, 2004.

Todd Huster, Jeremy Cohen, Zinan Lin, Kevin Chan, Charles Kamhoua, Nandi O Leslie, Cho-Yu Jason Chiang, and Vyas Sekar. Pareto gan: Extending the representational power of gans to heavy-tailed distributions. In *International Conference on Machine Learning*, pages 4523–4532. PMLR, 2021.

Priyank Jaini, Ivan Kobyzev, Yaoliang Yu, and Marcus Brubaker. Tails of lipschitz triangular flows. In *International Conference on Machine Learning*, pages 4673–4681. PMLR, 2020.

Hamid Jalalzai, Stephan Cléménçon, and Anne Sabourin. On binary classification in extreme regions. *Advances in Neural Information Processing Systems*, 31, 2018.

Richard W Katz, Marc B Parlange, and Philippe Naveau. Statistics of extremes in hydrology. *Advances in water resources*, 25(8-12):1287–1304, 2002.

Diederik P Kingma and Jimmy Ba. Adam: A method for stochastic optimization. *arXiv preprint arXiv:1412.6980*, 2014.

Diederik P Kingma and Max Welling. Auto-encoding variational bayes. *arXiv preprint arXiv:1312.6114*, 2013.

Mike Laszkiewicz, Johannes Lederer, and Asja Fischer. Marginal tail-adaptive normalizing flows. In *International Conference on Machine Learning*, pages 12020–12048. PMLR, 2022.

Yan Liu, Taha Bahadori, and Hongfei Li. Sparse-gev: Sparse latent space model for multivariate extreme value time serie modeling. *arXiv preprint arXiv:1206.4685*, 2012.

Linda Mhalla, Valérie Chavez-Demoulin, and Debbie J Dupuis. Causal mechanism of extreme river discharges in the upper danube basin network. *Journal of the Royal Statistical Society: Series C (Applied Statistics)*, 69(4):741–764, 2020.

Charlie Nash, Jacob Menick, Sander Dieleman, and Peter W Battaglia. Generating images with sparse representations. *arXiv preprint arXiv:2103.03841*, 2021.

Philippe Naveau, Armelle Guillou, and Théo Rietsch. A non-parametric entropy-based approach to detect changes in climate extremes. *Journal of the Royal Statistical Society: Series B (Statistical Methodology)*, 76(5):861–884, 2014.

Olivier C Pasche and Sebastian Engelke. Neural networks for extreme quantile regression with an application to forecasting of flood risk. *arXiv preprint arXiv:2208.07590*, 2022.

W Penny, S Kiebel, and K Friston. *Variational bayes*. Elsevier, London, 2006.

James Pickands III. Statistical inference using extreme order statistics. *the Annals of Statistics*, pages 119–131, 1975.

Ali Razavi, Aaron Van den Oord, and Oriol Vinyals. Generating diverse high-fidelity images with vq-vae-2. *Advances in neural information processing systems*, 32, 2019.

Sidney I Resnick. *Heavy-tail phenomena: probabilistic and statistical modeling*. Springer Science & Business Media, 2007.

Danilo Rezende and Shakir Mohamed. Variational inference with normalizing flows. In *International conference on machine learning*, pages 1530–1538. PMLR, 2015.

Danilo Jimenez Rezende, Shakir Mohamed, and Daan Wierstra. Stochastic backpropagation and approximate inference in deep generative models. In *International conference on machine learning*, pages 1278–1286. PMLR, 2014.

Théo Rietsch, P Naveau, N Gilardi, and Armelle Guillou. Network design for heavy rainfall analysis. *Journal of Geophysical Research: Atmospheres*, 118(23):13–075, 2013.

Holger Rootzén and Nader Tajvidi. Multivariate generalized pareto distributions. *Bernoulli*, 12(5):917–930, 2006.

Ethan M Rudd, Lalit P Jain, Walter J Scheirer, and Terrance E Boult. The extreme value machine. *IEEE transactions on pattern analysis and machine intelligence*, 40(3):762–768, 2017.

Gábor J Székely, Maria L Rizzo, and Nail K Bakirov. Measuring and testing dependence by correlation of distances. *The annals of statistics*, 35(6):2769–2794, 2007.

Phyllis Wan and Richard A Davis. Threshold selection for multivariate heavy-tailed data. *Extremes*, 22(1):131–166, 2019.

Xiaolei Xie. *Analysis of Heavy-Tailed Time Series*. PhD thesis, University of Copenhagen, Faculty of Science, Department of Mathematical …, 2017.

Tiancheng Zhao, Ran Zhao, and Maxine Eskenazi. Learning discourse-level diversity for neural dialog models using conditional variational autoencoders. *arXiv preprint arXiv:1703.10960*, 2017.

Chuanxia Zheng, Tat-Jen Cham, and Jianfei Cai. Pluralistic image completion. In *Proceedings of the IEEE/CVF Conference on Computer Vision and Pattern Recognition*, pages 1438–1447, 2019.